USGS
science for a changing world

Spatio-Temporal Evolution of Distributed Volcanic Fields, Case Studies—Sierra Chichinautzin and Michoacán-Guanajuato, México

Chapter I of
Distributed Volcanism—Characteristics, Processes, and Hazards

Professional Paper 1890

U.S. Department of the Interior
U.S. Geological Survey

Cover. Photograph showing the crater and lava flows of the Chichinautzin volcano (foreground). Monogenetic cones dot the background, and the polygenetic volcanoes Iztaccíhuatl and Popocatépetl can be seen through the clouds. Photograph by Amiel Nieto-Torres.

Spatio-Temporal Evolution of Distributed Volcanic Fields, Case Studies—Sierra Chichinautzin and Michoacán-Guanajuato, México

By Carmen Jaimes-Viera, Amiel Nieto-Torres, Ana Lillian Martin Del Pozzo, Aurelie Germa, Chuck Connor, Michael Ort, Paul Layer, and Jeff Benowitz

Chapter I of
Distributed Volcanism-Characteristics, Processes, and Hazards
Edited by Michael P. Poland, Michael H. Ort, Wendy K. Stovall, R. Greg Vaughan, Charles B. Conner, and M. Elise Rumpf

Professional Paper 1890

U.S. Department of the Interior
U.S. Geological Survey

U.S. Geological Survey, Reston, Virginia: 2025

Suggested citation:
Jaimes-Viera, C., Nieto-Torres, A., Martin Del Pozzo, A.L., Germa, A., Connor, C., Ort, M., Layer, P., and Benowitz, J., 2025, Spatio-Temporal Evolution of Distributed Volcanic Fields, Case Studies—Sierra Chichinautzin and Michoacán-Guanajuato, México, chap. I *of* Poland, M.P., Ort, M.H., Stovall, W.K., Vaughan, G.R., Conner, C.B., and Rumpf, M.E., eds., Distributed volcanism—Characteristics, processes, and hazards: U.S. Geological Survey Professional Paper 1890, 28 p., https://doi.org/10.3133/pp1890I.

ISSN 2330-7102 (online)

Contents

Abstract 1
Introduction 1
Geological Setting and Study Area 3
Sierra Chichinautzin Volcanic Field 3
Origin of Volcanism and Tectonic Setting 3
Eruptive Style and Volcanic Structures 5
Michoacán-Guanajuato Volcanic Field 5
Origin of Volcanism and Tectonic Setting 5
Eruptive Style and Volcanic Structures 5
Methodology 6
Volcano Distribution and Morphology 6
Cone Morphometry and Age Estimation 6
$^{40}Ar/^{39}Ar$ Geochronology 6
Kernel Density Analysis and Spline 7
Vent Cluster Agglomerative Hierarchical Dendrogram Analysis 7
Vent Alignment 7
Seismicity Analysis 8
State of the Plumbing System in the Sierra Chichinautzin Volcanic Field 8
Results 8
Sierra Chichinautzin Volcanic Field 8
Kernel Density Analysis 8
Geochronology and Spatial Distribution of Ages 8
Seismic Activity in the Sierra Chichinautzin Volcanic Field 11
State of the Plumbing System in the Sierra Chichinautzin Volcanic Field 12
Michoacán-Guanajuato Volcanic Field 12
Kernel Density Analysis 13
Vent Cluster Agglomerative Hierarchical Dendrogram Analysis 15
Cone Morphometry and Age Estimation 16
Seismic Activity in the Michoacán-Guanajuato Volcanic Field 17
Discussion 19
Density and Agglomerative Hierarchical Dendrogram Analysis 19
Geochronology and Spatial Distribution of Ages 19
Seismic Activity 20
Seismicity in Sierra Chichinautzin Volcanic Field 20
Seismicity in the Michoacán-Guanajuato Volcanic Field 20
State of the Plumbing System in the Sierra Chichinautzin Volcanic Field 21
Preparing for an Eruption 21
Conclusions 21
Acknowledgments 21
References Cited 22

Figures

1. Location map of the Sierra Chichinautzin and the Michoacán-Guanajuato volcanic fields in central Mexico....2
2. Maps outlining the Sierra Chichinautzin and Michoacán-Guanajuato volcanic fields....4
3. Map of the Sierra Chichinautzin volcanic field with corresponding rose diagrams....9
4. Graphs showing $^{40}Ar/^{39}Ar$ age spectra and isochron diagrams for samples from the El Cantil and the El Elefante volcanic features....10
5. Map showing the ages of the eruptions within the Sierra Chichinautzin volcanic field....11
6. Map showing the seismic activity within the Sierra Chichinautzin volcanic field....12
7. Map showing the position and trends of the feeder dikes in the Sierra Chichinautzin volcanic field....13
8. Map and rose diagrams showing kernel density analysis results of the Michoacán-Guanajuato volcanic field....14
9. Dendrogram representing the grouping of volcanoes within the Sierra Chichinautzin volcanic field....15
10. Histograms showing the distribution of the morphology of the Valle de Santiago....16
11. Map of the cone morphology within the Michoacán-Guanajuato volcanic field....17
12. Maps showing seismic activity in the Michoacán-Guanajuato volcanic field....18

Table

1. Summary of $^{40}Ar/^{39}Ar$ analyses in the Sierra Chichinautzin volcanic field....10

Conversion Factors

International System of Units to U.S. customary units

Multiply	By	To obtain
	Length	
meter (m)	3.281	foot (ft)
kilometer (km)	0.6214	mile (mi)
meter (m)	1.094	yard (yd)
	Area	
square kilometer (km^2)	247.1	acre
square kilometer (km^2)	0.3861	square mile (mi^2)
	Volume	
cubic kilometer (km^3)	264.2	billion gallons (Ggal)
cubic kilometer (km^3)	0.2399	cubic mile (mi^3)

Datums

Vertical coordinate information is referenced to the World Geodetic System 1984 (DWGS1984).

Horizontal coordinate information is referenced to the North American Datum 27 (NAD27).

Supplemental Information

E-notation is used in supplementary table 2 for values of isotopic ratios. For example, 1.0E+5 = 1×10^5.

Abbreviations

DEM	digital elevation model
ka	kilo-annum; thousands of years ago
k.y.	thousand years
Lidar	light detection and ranging
Ma	mega-annum; million years before present
m.y.	million years
MSWD	mean square weighted deviates
PCA	principal component analysis
USGS	U.S. Geological Survey

Distributed Volcanism—Characteristics, Processes, and Hazards
Edited by Poland, Ort, Stovall, Vaughan, Connor, and Rumpf
Professional Paper 1890

Chapter I

Spatio-Temporal Evolution of Distributed Volcanic Fields, Case Studies—Sierra Chichinautzin and Michoacán-Guanajuato, México

By Carmen Jaimes-Viera[1], Amiel Nieto-Torres[2], Ana Lillian Martin Del Pozzo[3], Aurelie Germa[1], Chuck Connor[1], Michael Ort[4], Paul Layer[5], and Jeff Benowitz[5]

Abstract

An analysis of 1,375 volcanoes in the Michoacán-Guanajuato (1,148 volcanoes in a 26,200 square-kilometer area) and Sierra Chichinautzin (227 volcanoes in a 3,500 square-kilometer area) volcanic fields in central Mexico identified patterns in the spatial and temporal distribution of past eruptions. A cluster agglomerative hierarchical method and kernel analysis confirmed that the Michoacán-Guanajuato volcanic field comprises four volcanic fields (Valle de Santiago, Uruapan, Apatzingán, and Pátzcuaro volcanic fields) controlled by different fault systems, indicating that it is not a single volcanic field but rather a group of volcanic fields (a "superfield"), each of which has distinct characteristics.

In the Sierra Chichinautzin volcanic field, well-constrained isotopic ages were used to build a model of how the spatial distribution of the eruptions has changed over time. Two new $^{40}Ar/^{39}Ar$ ages from a locally recognized volcanic feature near the town of El Cantil, herein called El Cantil volcano (1,537±17 kilo-annum [ka]) and the volcanic feature at Cerro el Elefante (herein called El Elefante dome) (1,485±92 ka) belong to the oldest volcanic group identified in the Sierra Chichinautzin volcanic field, confirming the timing of the beginning of monogenetic volcanism in the region. Based on the volcanic groups identified in the Sierra Chichinautzin volcanic field, the youngest volcanism (less than 35 ka) is found only in the central-western sector of the field. Principal component analysis determined the directional trends of feeder dikes only for vents <10 ka in the Sierra Chichinautzin volcanic field. Possible magma migration paths through the crust were identified using seismic data from both volcanic fields using an earthquake catalog from 1973 to 2023, which includes 9,016 earthquakes in the Michoacán-Guanajuato volcanic field and 841 in the Sierra Chichinautzin volcanic field. The spatial distribution of the hypocenters does not highlight any trend that could be associated with superficial movement of magma in the Sierra Chichinautzin volcanic field. In the Michoacán-Guanajuato volcanic field, however, eight seismic swarms since 1997 have been detected. These swarms are interpreted to result from ascending magma. Strengthening monitoring systems and reinforcing mitigation measures to address volcanic hazards and risk are important means of preparing for future eruptions in both regions. Analysis such as those herein provide insights as to where an eruption might occur and may help mitigate volcanic hazards.

Introduction

Recognizing spatial patterns in distributed volcanism is an important task in determining future hazards and risk in distributed volcanic fields. Because of the large extent of many distributed volcanic fields—as much as thousands of square kilometers with tens to hundreds of eruptive vents—the location of the next eruption is difficult to forecast. Identifying how and when such volcanism has occurred in the past within a volcanic field and establishing the spatial extent of the volcanism through time and space provides valuable information related to the hazards and risks associated with future eruptions.

Spatial and temporal pattern recognition of vent distribution can aid with estimating probabilities of occurrence of an eruption in time and space (Scandone, 1979; Connor and Hill, 1995; Connor and Conway, 2000; Alberico and others, 2002; Bebbington, 2013; Sobradelo and others, 2014, Nieto-Torres and Martin Del Pozzo, 2019). The most used method to estimate hazard in a distributed volcanic field is kernel density estimation, where the spatial variation in the number of volcanoes per square kilometer is estimated as a function of the distance between volcanoes using kernel functions (Nieto-Torres and Martin Del Pozzo, 2019). One of the first investigations of spatial distribution with kernel density methods was carried out in some volcanic fields in the Trans-Mexican volcanic belt by Connor (1990). Kernel density methods have been improved since then, mainly by the modification of the selection algorithm of the search

[1]University of South Florida

[2]Millennium Institute on Volcanic Risk Research

[3]Universidad Nacional Autónoma de México

[4]Northern Arizona University

[5]University of Alaska

radius, but also by integrating additional data such as seismicity or slowness in seismic velocity (Kiyosugi and others, 2010). Quantum Geographic Information System (QGIS) software for volcanic susceptibility, called QVAST, was developed by Bartolini and others (2013) to construct a probabilistic density function using a kernel density estimator, as well as to generate quantitative assessments of the probability of a new eruptive vent forming in a given area (Bartolini and others, 2017).

Because monogenetic volcanic fields evolve over time, eruption locations vary owing to changes such as tectonic stress and magma source region. Estimations of volcanic hazards therefore need to consider the age distributions of the eruptions across the field and tectonic features, such as faults and fractures—especially those associated with the most recent eruptions (Nieto-Torres and Martin Del Pozzo, 2019). Pre-existing faults or fractures can control magma intrusions and their propagation through the crust (Delaney and others, 1986; Connor and others, 2000; Kósik and others, 2020). Faults are zones of crustal weakness that magma uses during ascent, influencing the spatial distribution of monogenetic volcanoes (Delaney and others, 1986; Johnson and Harrison, 1989; Bevilacqua and others, 2017). Consequently, the location of recent seismic events, whether associated with magma intrusion or with fault slip, can be used as additional information regarding where future vents may form within distributed volcanic fields.

Distributed volcanism is thought to be basaltic (sometimes including more siliceous compositions), low-volume, and short-lived (for example, Cañón-Tapia and Walker, 2004; Smith and Németh, 2017). However, these ideas are not entirely consistent with the distributed volcanism of the Trans-Mexican volcanic belt.

In the Sierra Chichinautzin volcanic field (fig. 1), south of Mexico City, the basaltic to andesitic eruptions (<35 kilo-annum [ka]) lasted from months to tens of years and had lava volumes of up to 6 cubic kilometers (km^3) (Nieto-Torres and others, 2023). Several eruptions in the Sierra Chichinautzin volcanic field affected the area where Mexico City is located today (Martin Del Pozzo, 1982; Cordova and others, 1994; Martin Del Pozzo and others, 1997). Lava from a volcanic feature locally called Xitle volcano flowed into the then inhabited southern Mexico City, burying most parts of the Cuicuilco Pyramid archaeological site (Cordova and others, 1994). Ages for this eruption are based

Figure 1. Map showing the tectonic setting of the study area and the locations of the Sierra Chichinautzin and the Michoacán-Guanajuato volcanic fields in central Mexico.

on charcoal found beneath the flow (about 2,000 years before present [1950]) and on paleomagnetism, archaeomagnetism, and dated charcoal (about 1,670 years before present) (for example, Cordova and others, 1994, Urrutia-Fucugauchi, 1996; Böhnel and others, 1997; Morales and others, 2014; Alva-Valdivia, 2005; Urrutia-Fucugauchi and others, 2016; Cervantes-Solano and others, 2019). Chichinautzin Volcano, which may be the youngest in this field, has been dated at 1,835 years before present (Siebe and others, 2004) but may have formed as recently as about 1,600 years ago (Blanco and Guilbaud, 2025). Its name, which means "Burning Lord" in the Náhuatl language, suggests that the eruption was witnessed by the Indigenous people of the region. Fluid lava flows are evident in all directions from the volcano; some flows would have reached sparsely populated areas near what is now Mexico City (Martin Del Pozzo and others, 1997, Nieto-Torres and others, 2023).

In the Michoacán-Guanajuato volcanic field (fig. 1), recent basaltic to andesitic eruptions (<10 ka) have emitted an average of <1 km^3 of lava and lasted for years. For example, Parícutin, which started erupting in 1943 and was active for 9 years; and Jorullo, which began erupting in 1759 and was active for 15 years. Eruptions with total volumes of lava up to 9 km^3 are estimated to have lasted as long as 30 years (Chevrel and others, 2016). The Michoacán-Guanajuato volcanic field historical eruption of Jorullo volcano demonstrates the effects that even small-volume eruptions (<1 km^3) can produce (Nieto-Torres and others, 2023). The tephra (lapilli and ash fallout) and lava flows of the Jorullo eruption in 1759 covered ~9 square kilometers (km^2), which destroyed nearby farmlands and forced the evacuation of the sugar cane haciendas (Orozco and Berra, 1854). The tephra fallout from the Parícutin eruption in 1943 completely covered farmland up to 26 kilometers (km) away from the vent, and distal ash was reported as far as Mexico City and Guadalajara, while the lava flows caused the abandonment and destruction of the town of San Juan Parangaricutiro (Martin Del Pozzo and others, 1997).

Future volcanism in either of these two volcanic fields may have greater effects because the areas are now more densely populated. In this paper, we present an analysis of the volcanic activity in space and time in these two Mexican volcanic fields (Sierra Chichinautzin and Michoacán-Guanajuato volcanic fields), using isotopic age determinations, stratigraphy, chemical data, cone morphology, and spatial analysis to understand the distribution patterns that will help to constrain volcanic hazard and risk.

Geological Setting and Study Area

The Trans-Mexican volcanic belt is the result of the subduction of the Cocos and Rivera Plates beneath the North America Plate at the Middle America Trench (fig.1) since the Miocene (Nixon, 1982; Johnson and Harrison, 1990; Pardo and Suárez, 1995; Pérez-Campos and others, 2008; Ferrari and others, 2012, 2018). The entire Trans-Mexican volcanic belt is over 1,000 km long, which stretches east-west across south-central Mexico, including through heavily populated areas like those around Mexico City. The complex tectonic setting off the west coast of Mexico includes both spreading centers in the north and subduction zones in the south, and consists of more than 3,000 volcanoes (Connor, 1990). The Trans-Mexican volcanic belt has a complex tectonic history. The volcanic arc is subparallel to the trench because of the geometry of the subducting Cocos Plate. Geophysical studies of the Trans-Mexican volcanic belt show that the Cocos Plate is sub-horizontal near the trench, and as it moves inland it steepens to subduct almost vertically, reaching a depth of about 150 km under Mexico City (Pérez-Campos and others, 2008). The Cocos Plate has an oblique subduction angle with respect to the Middle America Trench, subducting towards the north-northeast (Pardo and Suárez, 1995; Ferrari and others, 1999). Geologic evidence indicates that the Trans-Mexican volcanic belt is presently under an extensional tectonic regime that has a small and variable left-lateral component (Pasquarè and others, 1990, 1991; Gómez-Tuena and others, 2008) that may be explained by the small degree of obliquity of the convergence between the Cocos and North America Plates (Mazzarini and others, 2010). The gap between the Middle America Trench and the volcanic front is about 400 km in the east, and it decreases to 200 km as it moves westward, consistent with changes in the dip angle of the deep seismic zone and the convergence rate of the Cocos and North America Plates (Burbach and others, 1984).

The Sierra Chichinautzin volcanic field (fig. 2*A*) contains about 227 volcanic vents in an area of 3,500 km^2 and is in southern Mexico City—an active volcanic field in an urban environment. The volcanic field is bordered to the east by the Popocatépetl and Iztaccihuatl volcanoes, and to the west by the Pliocene and Pleistocene polygenetic andesitic volcanoes belonging to the Las Cruces and Zempoala ranges (Delgado-Granados and Martin Del Pozzo, 1993; Arce and others, 2013). Farther west, another field of monogenetic cones, called the Tenango volcanic field, is sometimes referred to as part of the Sierra Chichinautzin volcanic field (Bloomfield, 1975). We consider it to be an independent field because it is morphologically separated from the Sierra Chichinautzin volcanic field by larger mountains. The Sierra Chichinautzin volcanic field is bordered to the north by the lacustrine sediments of the ancient lakes that form the Valle de México (herein called Basin of México).

Sierra Chichinautzin Volcanic Field

Origin of Volcanism and Tectonic Setting

The origin of volcanism in the Sierra Chichinautzin volcanic field is debated. Some authors suggest that because volcanism in the Sierra Chichinautzin volcanic field is predominantly andesitic, with some basaltic and dacitic lava flows and vents, with calc-alkaline and alkaline affinity, the field is associated with subduction processes (Negendank, 1972; Martin Del Pozzo, 1982, 1990; Wallace and Carmichael, 1999; Martínez-Serrano and others, 2004). Márquez and others (1999) and Verma (2000) related the volcanism to intraplate magmatism. Unlike other authors, Verma (2000) interpreted, through isotopic and geochemical analysis, that volcanism in the Sierra Chichinautzin

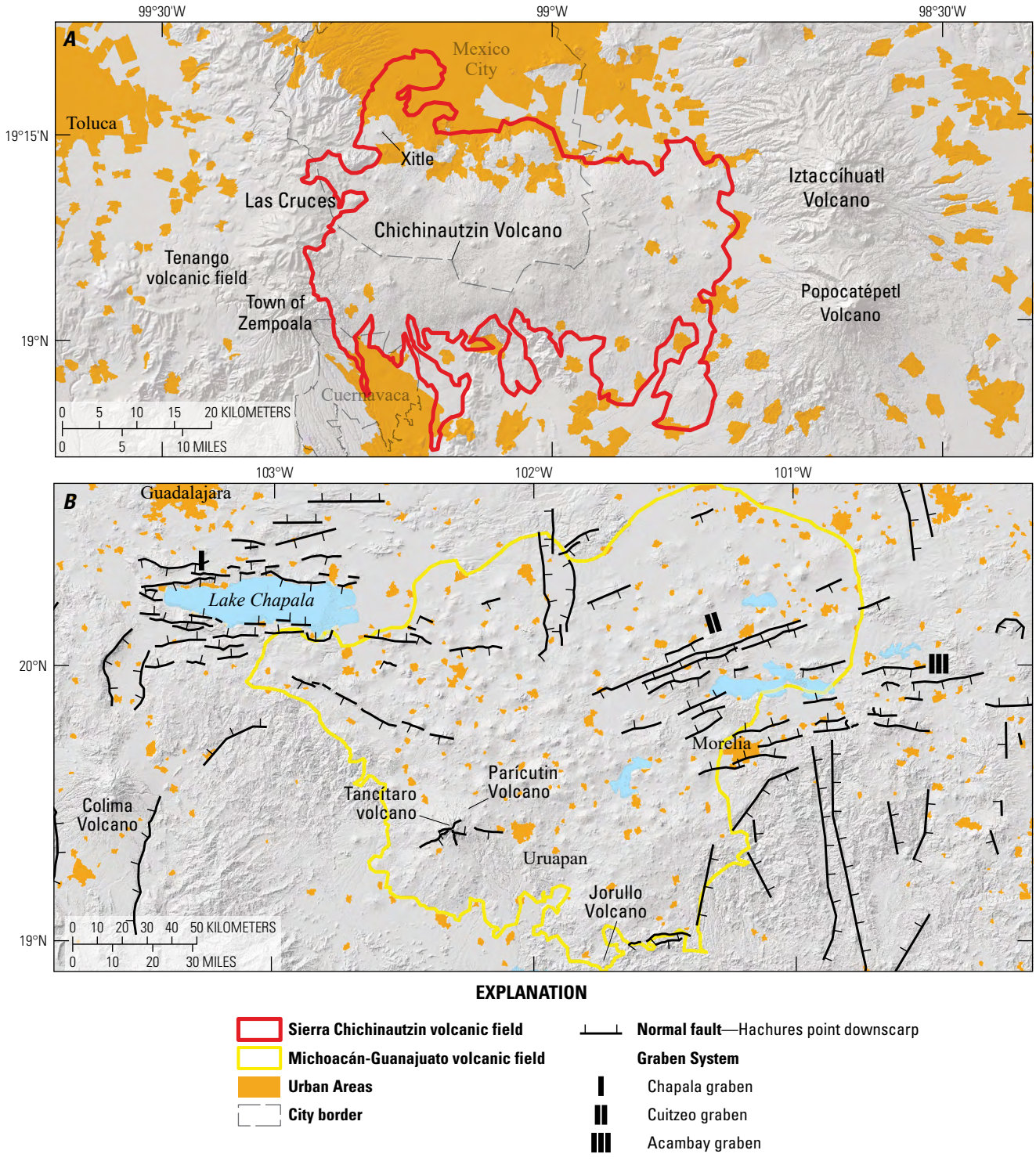

Figure 2. Maps outlining the Sierra Chichinautzin and Michoacán-Guanajuato volcanic fields. *A,* Outline of the Sierra Chichinautzin volcanic field and the surrounding volcanic features. *B,* Outline of the Michoacán-Guanajuato volcanic field and the surrounding graben systems.

volcanic field is probably generated in an extensional environment via partial melting of the mantle. Straub and Martin Del Pozzo (2001), Cervantes and Wallace (2003), and Straub and others (2008) related the origin of the magmas to partial melting and fractional crystallization above the asthenospheric wedge. In addition, they proposed that Sierra Chichinautzin volcanic field magmas evolve in the mantle and lower crust because of crustal contamination and magma mixing.

Monogenetic volcanoes in the Sierra Chichinautzin volcanic field are aligned in an east-west direction (fig. 3; Bloomfield, 1975; Martin Del Pozzo, 1982; Martin Del Pozzo and others, 1997; Alaniz-Álvarez and others, 1998; Márquez and others, 1999), and the volcanic field is coincident with a series of east-west trending faults. The faults are apparent in the height difference between the Mesozoic limestone rocks in the Basin of México at ~1,000 meters (m) above sea level (Morales-Casique and others, 2018) and those to the south towards the town of Cuernavaca, where they crop out at 1,500 meters above sea level. Thus, the Sierra Chichinautzin volcanic field is located along a regional normal fault (Márquez and others, 1999; Ferrari and others, 1994, Ferrari and others, 2000). Alaniz-Álvarez and Nieto-Samaniego (2005) named this major fault system La Pera, and it may be an extension of the Tenango Fault system, located to the west (fig. 3, García-Palomo and others, 2002, 2008; Norini and others, 2006). The Tenango Fault system has typical deformation for a transtensional stress regime, with left-lateral kinematics and a normal component, and it follows a general east-west trend that passes through the Nevado de Toluca volcano. The fault system consists of two main sets of faults; the first running east-west to the east of Nevado de Toluca, whereas the other set runs from east-southeast to west-northwest on the west side of Nevado de Toluca (Norini and others, 2006). Based on volcanic alignments in the area, the Xochimilco and Xicomulco Faults run east-west, along the slope of the Basin of México (Martin Del Pozzo, 1981).

Eruptive Style and Volcanic Structures

The eruptive style at the Sierra Chichinautzin volcanic field is mainly Strombolian, although some violent Strombolian to Hawaiian-type eruptions have been observed. Some Santiaguito type eruptions have occurred, which are characterized by the emission of thick lava flows (150 to 300 m) typically observed at Santiaguito volcano in Guatemala since 1922 (Rose, 1973). Phreatic eruptions are rare in this volcanic field (Nieto-Torres and others, 2023).

Bloomfield (1975) and Martin Del Pozzo (1982) defined three main types of structures within the Sierra Chichinautzin volcanic field: 1. Scoria cones with lava flows, such as Xitle volcano, which are characterized by having external slopes of 30 degrees; 2. shield volcanoes crowned with a scoria cone, such as Chichinautzin Volcano (also known as Mexican shield volcanoes); 3. coneless lava flows that are between 70 and 300 meters thick and have an andesitic-dacitic composition. Examples of this latter, Santiaguito-type of structure are Tetequillo and Xicomulco (Nieto-Torres and others, 2023).

Michoacán-Guanajuato Volcanic Field

The Michoacán-Guanajuato volcanic field (fig. 2*B*) is a late Pliocene to Quaternary volcanic field in the central portion of the Trans-Mexican volcanic belt, that is bordered on the west by the Colima volcano. It is considered one of the largest and most diverse distributed volcanic fields in the world that is related to a subduction tectonic setting (Connor, 1987; Valentine and Connor, 2015), with more than 1,148 volcanic vents in an area that previously was estimated at 40,000 km^2 (Hasenaka and Carmichael, 1985a, 1985b). We have reassessed this area to be 26,209 km^2 based on recent digital elevation models, satellite imagery, and topography.

Origin of Volcanism and Tectonic Setting

The magmatism of the Michoacán-Guanajuato volcanic field began in the Pliocene epoch (5 million years ago [Ma]), but there is evidence that its activity increased in the Quaternary period, and it is possible to identify a clear migration trend toward the southwest (3–2.58 Ma to present; Hasenaka and Carmichael 1985a, 1985b; Murphy, 1986; Ban and others, 1992). Also, some authors have proposed that the Michoacán-Guanajuato volcanic field is subdivided into four different zones through a kernel vent clusters analysis (Connor, 1990; Mazzarini and others, 2010). The Michoacán-Guanajuato volcanic field rocks have a calc-alkaline signature (Hasenaka and Carmichael, 1987; Gómez-Tuena and others, 2008). The central Mexican arc in the Michoacán-Guanajuato region is in an extensional tectonic regime, and in this area the graben system from west to east consists of: Chapala graben, Cuitzeo graben, and Acambay graben (fig. 2; Kurokawa and others, 1995). Extension in the volcanic field occurs in a north-northwest direction (Suter and others, 2001), and the crust is about 35 km thick (Urrutia-Fucugauchi and Flores-Ruiz, 1996). The subducting slab of the Cocos Plate is about 80–100km deep in this region (Pardo and Suárez, 1995). The volcanism of the Michoacán-Guanajuato volcanic field is probably generated by the partial melting of a heterogeneous mantle contaminated with subducted sediments and oceanic crust, partial melting of the deep crust, fractional crystallization and assimilation and fractional crystallization processes (Luhr and Carmichael, 1985; McBirney and others, 1987; Agrawal and others, 2008; Johnson and others, 2008; Cebriá and others, 2011; Ownby and others, 2011).

Eruptive Style and Volcanic Structures

The eruptive style that we can find in the Michoacán-Guanajuato volcanic field are strombolian, effusive, and phreatomagmatic activity, includes a wide variety of volcanic landforms, like scoria/spatter cones with or without associated lava flows, small-to-medium-sized shield volcanoes (“Mexican shields”; Hasenaka and others, 1994),

fissure-fed lava flows and lava domes, phreatomagmatic volcanoes (maars, tuff rings, and tuff cones), and only two extinct stratovolcanoes (Patambán and Tancítaro; Ownby and others, 2007).

Approximately 90 percent of volcanoes within the Michoacán-Guanajuato volcanic field are basaltic monogenetic cinder cones but we can find andesitic to dacitic compositions (Hasenaka and Carmichael, 1985a, 1985b, 1987; Ban and others, 1992; Hasenaka and others, 1994).

Methodology

Volcano Distribution and Morphology

For our analysis, we define a volcanic event as a continuous eruption in time and space; an independent eruption center defines a single-vent event, and crater rows and overlapping cones represent a multiple-vent event (Runge and others, 2014). We constrained volcanic events using two parameters: the eruption age and the direction of the major semi-axis of the cone base. Cones with different *h/wb* ratio (where *h* is height and *wb* is basal diameter) and (or) different ellipsoid direction were recorded as different eruptions (Nieto-Torres and Martin Del Pozzo, 2019). Hornitos and rootless vents were omitted to avoid overvaluing the analysis as found in Becerril and others (2013).

For both of the volcanic fields, the identification and the distribution of the volcanic events, tectonic features such as faults, fissures and volcano alignments, as well as the cone morphometric parameters *h* and *wb* of the cones, were measured using Sentinel 2 satellite images, vertical aerial photographs at 1:15,000 scale, topographic maps (National Institute of Statistics and Geography 1:20,000 scale) and a 5 m light detection and ranging (lidar) digital elevation model, confirmed by field work at more than 300 sites. The basal diameter of each cone, *wb*, was obtained from the average between the semi-major and semi-minor axes because many cones have an elliptical base instead of a circular base. The height was measured with profiles of the cone using ArcGIS (version 10.3, https://www.esri.com/en-us/home) on two digital elevation maps, one of 15 m resolution and the second of 5 m resolution. We considered the difference between the lowest-level curve, belonging to the base of the cone, and the highest-level curve, belonging to the crater, for the height, as in Nieto-Torres and Martin Del Pozzo (2019). Lava flows with no associated cone were treated separately; their aspect ratio was calculated by measuring the thickness, length, ridges, as well as soil thickness covering the flows, and all these characteristics were considered to estimate the age using the morphological criteria of Martin Del Pozzo (1982). For the Michoacán-Guanajuato volcanic field, we also integrated some distribution and geomorphometric parameters from previous studies of Hasenaka and Carmichael (1985a, 1985b) and Connor (1990).

Cone Morphometry and Age Estimation

The *h/wb* ratio was used to determine the degree of cone erosion over time for the cones of each volcanic field. This parameter is considered useful in assessing the relative ages of the cones within a volcanic field if erosion rates are reasonably consistent across the area (Wood, 1980; Hooper, 1995; Inbar and others, 2011, Dóniz-Páez, 2015; Bemis and Ferencz, 2017; Jaimes-Viera and others, 2018, Nieto-Torres and Martin Del Pozzo, 2019). We applied this criterion in the Michoacán-Guanajuato volcanic field, because the field is located within the same latitudinal band where climatic conditions do not have much variation. For the Sierra Chichinautzin volcanic field, we calibrated the morphometric data with chronological data that were published previously (Jaimes-Viera and others, 2018 and references therein). The cones were reclassified according to cone morphology from youngest to oldest. We also considered the preservation of lava flows including features such as flow margins, thickness of soil cover, and pressure ridges, using the morphological criteria of Martin Del Pozzo (1982).

$^{40}Ar/^{39}Ar$ Geochronology

Two samples from the Sierra Chichinautzin volcanic field were analyzed at the geochronology laboratory of the University of Alaska, Fairbanks, following the methodology used in Jaimes-Viera and others (2018). The monitor mineral TCR-2 with an age of 28.616 Ma (Renne and others, 1994, 2010) was used to monitor neutron flux and calculate the irradiation parameter, *J*, for both samples. The monitors were fused, and the samples were heated using a 6-watt argon-ion laser following the techniques described in York and others (1981), Layer and others (1987), and Benowitz and others (2014). The argon isotopes measured were corrected for system blank and mass discrimination, as well as calcium, potassium and chlorine interference reactions following procedures outlined in McDougall and Harrison (1999). Typical full-system 8 minutes laser blank values (in moles) were generally 2×10^{-16} mol ^{40}Ar, 3×10^{-18} mol ^{39}Ar, 9×10^{-18} mol ^{38}Ar and 2×10^{-18} mol ^{36}Ar, which are 10–50 times smaller than the sample/standard volume fractions. Correction factors for nucleogenic interferences during irradiation were determined from irradiated CaF_2 and K_2SO_4 as follows: $(^{39}Ar/^{37}Ar)$ $Ca = 7.06 \times 10^{-4}$, $(^{36}Ar/^{37}Ar)$ $Ca = 2.79 \times 10^{-4}$ and $(^{40}Ar/^{39}Ar)$ $K = 0.0297$. Mass discrimination was monitored by running calibrated air shots and a zero-age glass sample. The mass discrimination during these experiments was 0.8 percent per mass unit. A sample is considered to have a plateau if it has three or more contiguous fractions constituting at least 50 percent ^{39}Ar release and is significant at the 95 percent confidence level (as indicated by a Mean Square Weighted Deviates; MSWD <~2.5). A sample is considered to form an isochron if it has three or more contiguous fractions that form a linear array that is significant at the 95 percent confidence level (MSWD <~2.5). All ages were quoted to the ±1 sigma level and calculated using the constants of Renne and others (2010). The integrated age is the age given by the total gas measured

and is equivalent to a potassium argon (K-Ar) age. The spectrum provides a plateau age if three or more consecutive gas fractions represent at least 50 percent of the total gas release and are within two standard deviations of each other (MSWD <~ 2.5).

For the Sierra Chichinautzin volcanic field, 2 new $^{40}Ar/^{39}Ar$ ages for El Elefante and El Cantil volcanoes, 24 $^{40}Ar/^{39}Ar$ ages from Jaimes-Viera and others (2018), and 23 previous ^{14}C and $^{40}Ar/^{39}Ar$ ages were integrated to provide a total of 49 radiometric ages (supplementary table 1). We also integrated 136 estimated ages calculated with a morphometric-based age model calibrated with radiometric dating (^{14}C and $^{40}Ar/^{39}Ar$, see supplementary table 1; Nieto-Torres and Martin Del Pozzo, 2019) in order to classify the volcanoes into different age groups. The two new ages in Sierra Chichinautzin volcanic field are important because they support the idea that the beginning of the monogenetic volcanism in this area was about 1.5 Ma, being older than previously thought, and also support that the location for the initial volcanic manifestations were in the northern part of the volcanic field. We therefore consider the temporal and spatial evolution of the Sierra Chichinautzin volcanic field to be reasonably well constrained.

Kernel Density Analysis and Spline

A kernel density analysis was performed to analyze the density of vents considering their spatial distribution. We used a uniform kernel within a search radius, *r*, centered on each vent in the dataset. The length of the search radius strongly controls the final pattern of the density distribution—the higher the r value, the smoother the resulting pattern in the spatial density model. For the Michoacán-Guanajuato volcanic field we used *r*=15 km, and for the Sierra Chichinautzin volcanic field we used *r*=9 km. These two radii are the distance of the most isolated volcano to its nearest neighbor in each volcanic field (Nieto-Torres and Martin Del Pozzo, 2019)—that is, the radius is chosen as the minimum radius that avoids isolated clusters consisting of only one vent.

In the case of the Sierra Chichinautzin volcanic field, where the ages and the temporal evolution of the field are better constrained, we made a geostatistical analysis of the ages using the Spline method (which uses estimated values in a mathematical function to minimize the overall curvature of the surface, resulting in a smooth surface that passes exactly through the input points). A raster surface was interpolated from points using a two-dimensional minimum curvature spline technique. The resulting smooth surface was useful to determine the temporal distribution of the cones in the study area (Jaimes-Viera and others, 2018).

Vent Cluster Agglomerative Hierarchical Dendrogram Analysis

The spatial distribution of vents in the Michoacán-Guanajuato volcanic field and the Sierra Chichinautzin volcanic field was investigated through a machine learning algorithm called the agglomerative hierarchical method, implemented using R Hierarchical Clustering v1.0.5 (Wessa, 2023). The clustering of the 1,148 Michoacán-Guanajuato volcanic field and 227 Sierra Chichinautzin volcanic field vents was calculated using the Manhattan Distance, in which the distance between two points is defined as the sum of the absolute differences of their coordinates. The Manhattan Distance was used in the complete-linkage clustering method to define the distance between two or more clusters. This method considers the maximum distance between clusters, taking into account all vents in one cluster and all vents in the other clusters. The optimal number of clusters is obtained by analyzing a dendrogram that represents the combination of all vents within clusters. Each vent in the dataset is assigned to a proper cluster that is characterized by the number of vents, the average distance of all the vents within the cluster from the centroid, and the location of the centroid. The cluster similarity is defined as the percent of the minimum distance at a given step relative to the maximum distance between the vents (Mazzarini and others, 2010).

Complete-linkage clustering is one of several methods of agglomerative hierarchical clustering. At the beginning of the process, each vent is in a cluster of its own. The clusters are then sequentially combined into larger clusters until all vents end up being in the same cluster. The method is also known as farthest neighbor clustering. The result of this clustering can be visualized as a dendrogram, which shows the sequence of cluster fusion and the distance at which each fusion took place. Mathematically, the complete linkage function between clusters A, B, C, E and F and [d (A, B, C, E, F)] is described by the following expression:

$$\max_{a\in A,\ b\in B,\ c\in C,\ e\in E,\ f\in F} d(a,b,c,e,f), \tag{1}$$

where:

d (a, b, c, e, f) is the distance between elements a ∈ A, b ∈ B, c ∈ C, e ∈ E, and f ∈ F, and

a ∈ A is the element "a" that belongs to the cluster A and so on.

Vent Alignment

An analysis of vent alignments was done for the Michoacán-Guanajuato volcanic field using the three-point alignments method proposed by Le Corvec and others, (2013) in which the alignment is valid only if the three points (vents) are within a predetermined tolerance. This method is commonly used to determine the preferred orientation of volcanic cone alignments and is useful to detect faults and fissures. This method was used to help discriminate between the different fault systems and identify vent clusters that could indicate groupings of volcanoes with different orientations, which allowed for the identification of distinct volcanic groups in both, Sierra Chichinautzin and Michoacán-Guanajuato volcanic fields.

Seismicity Analysis

Seismic information for both volcanic fields was compiled and integrated from the seismic network of the Universidad Nacional Autónoma de Mexico-Servicio Sismológico Nacional (UNAM-SSN). This 50-year catalog (1973 to 2023) contains information on date, time, magnitude, latitude, longitude, and depth for 9,016 events in the Michoacán-Guanajuato volcanic field and 841 in the Sierra Chichinautzin volcanic field (UNAM-SSN, 2023). This information allowed us to assess the behavior of earthquakes in both fields and helped differentiate deep earthquakes (>50 km), possibly associated with plate tectonic events, from shallow ones (<50 km) that might be related to slip on crustal faults or magma trapped in the crust for variable periods of time before its eventual eruption at the surface (Legrand and others, 2023).

State of the Plumbing System in the Sierra Chichinautzin Volcanic Field

The analysis of the shape of volcanic clusters provides information about a volcanic field's plumbing system. Furthermore, the azimuth of the maximum axis of the standard deviational ellipse allows us to identify directional trends and can be used as a proxy for the elongation of the feeder dikes at depth beneath the volcanic field (Le Corvec and others, 2013; Mazzarini and others, 2016).

Principal component analysis (PCA) is a linear method for dimensionality reduction that allows shape and direction of an x,y variable to be estimated by providing the eccentricity (shape) and azimuth (direction) parameters (Mazzarini and others, 2016). Eccentricity is defined from the lengths of the first and second eigenvectors of a length and width covariance matrix and varies between 0 and 1. A value of eccentricity close to 0 is expected for a circle, whereas values close to 1 represent an elongate ellipse (Mazzarini and others, 2016). The azimuth of the first eigenvalue of a covariance matrix (that is, the direction of the first eigenvector) represents the trend of the long axis of the ellipse that fits the trend of the volcanic clusters and can be used as a proxy to infer the shape of the feeder dikes beneath the volcanic field (Connor and others, 1992; Paulsen and Wilson, 2010; Rooney and others, 2011; Le Corvec and others, 2013; Muirhead and others, 2015; Mazzarini and others, 2016).

To perform the PCA, we carried out a directional distribution (standard deviational ellipse) analysis in ArcGIS 10.3, which solves the PCA matrix, calculating the eigenvalues and eigenvectors (Mitchell and Griffin, 2005). Monogenetic volcanoes of the Sierra Chichinautzin volcanic field younger than 10 ka were analyzed because the spatial and temporal distribution of these volcanoes are well constrained (for example, Jaimes-Viera and others, 2018; Nieto-Torres and Martin Del Pozzo, 2019; Nieto-Torres and others, 2023).

In addition to the above, we performed an analysis of the trend of faults, fissures and vent alignments between clusters using rose diagrams of those tectonic elements. This analysis has been used to determine the presence of potential faults where magma rose. It can also be used to identify groups with different trends that would indicate different fault or fracture systems and vent distribution, thus allowing for the proposal of distinct groups of volcanoes within a given volcanic field.

Results

Sierra Chichinautzin Volcanic Field

In this section we will show how the data obtained, in the different analyses we have done, describe the distribution and behavior of the volcanic field through time and space.

Kernel Density Analysis

The 9 km search radius used for the uniform kernel in the Sierra Chichinautzin volcanic field produced a main, east-northwest trending cluster of volcanoes in the central part of the field that corresponds to the trend of regional faulting. The total number of vents is 227 in an area of 3,500 km^2, and the average density for the whole field is 0.064 vents/km^2. The highest concentration of volcanic vents occurs in the central part of the main cluster (0.278 vents/km^2), decreasing towards the limits of the field, with a noticeably lower concentration in the eastern, southern, and northern parts of the volcanic field, including in the vicinity of Cuernavaca and within Mexico City (fig. 3*A*). The analysis of the faults, fissures, and vent alignments in the Sierra Chichinautzin volcanic field show that the trend is mainly east-west, from 70 degrees to 115 degrees (fig. 3*B*).On the other hand, when eruptions of the last 10 thousand years (k.y.) are analyzed, we found that the most recent eruptions are located in the central and western parts of the field. Notably, only eruptions older than 10 ka are identified in the eastern part of the field, in the vicinity of the Popocatépetl volcano. The volcanoes in this eastern part are covered by tephra and some reworked deposits from Plinian eruptions of Popocatépetl that were dated at about 23 ka (Tochimilco pumice, also called White Pumice; Espinasa-Pereña and Martin Del Pozzo, 2006, Siebe and others, 2017). These reworked deposits from Plinian eruptions of Popocatépetl are also observed towards the clusters to the north and south of the field (figs. 3*A* and 5).

Geochronology and Spatial Distribution of Ages

In the Sierra Chichinautzin volcanic field, the ages of the eruptions are well constrained (Jaimes-Viera and others, 2018; Nieto-Torres and Martin Del Pozzo, 2019), which helped us to identify three volcanic groups (older, intermediate, and younger volcanism) inside this volcanic field. This information was used to build a model of the spatial distribution of eruptions over time. The oldest volcanism, with ages about 1,537 and 765 ka, is located in the southern and northern parts of the field, respectively, with a north-northeast to south-southwest orientation of the vents

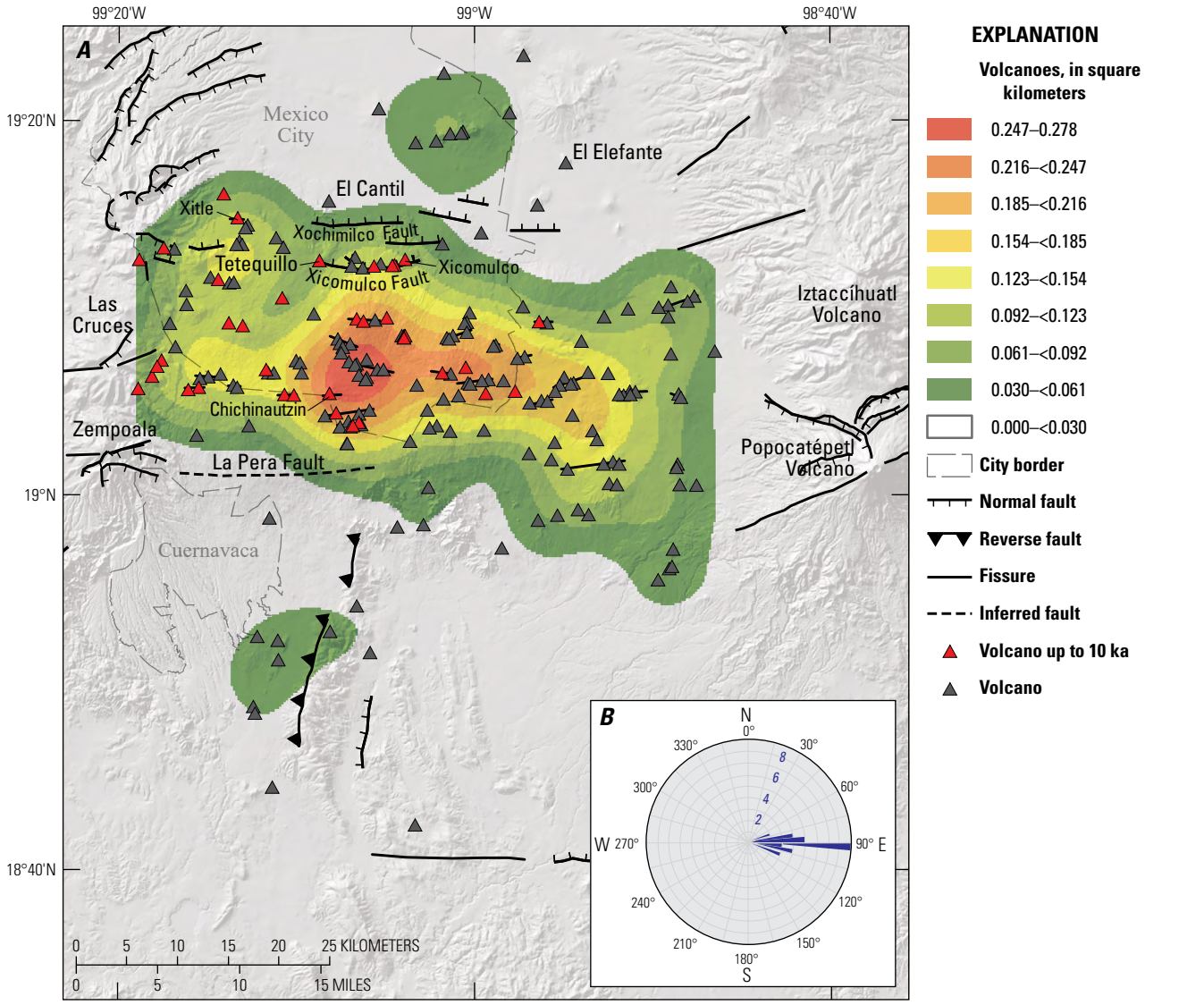

Figure 3. Map of the Sierra Chichinautzin volcanic field with corresponding rose diagrams. *A*, Kernel density results of the Sierra Chichinautzin volcanic field using a uniform kernel (where the radius is 9 kilometers). Highest concentration of volcanoes is found in the central part of the area. Areas with concentration of volcanoes per square kilometer less than 0.030 have no color. The two newest volcanic features, El Cantil (1,537±17 thousand years ago) and El Elefante (1,485±92 thousand years ago), are in the northern part of the volcanic field. *B*, Rose diagrams for the fault azimuthal trend direction in the Sierra Chichinautzin volcanic field. Numbers indicate the number of faults or fissures in that direction.

(fig. 5). The most recent features within the older volcanism group (table 1, fig. 4) belong to the volcanic feature at Cerro el Elefante (herein called El Elefante dome) (1,485±92 ka) and the volcanic feature at the town of El Cantil (herein called El Cantil volcano) (1,537±17 ka). Both volcanoes are located in the northern part of the Sierra Chichinautzin volcanic field (figs. 3*A* and 5).

The second period of volcanic activity in Sierra Chichinautzin volcanic field is thought to have occurred between 238 and 85 ka and is distributed both in the central part and towards the edges of the field (Jaimes-Viera and others, 2018). The vent alignments of the second stage are northeast-southwest and are separated from the oldest volcanism (fig. 5). The youngest volcanism (Younger Chichinautzin volcanic field) began at 35 ka, and it is found in the central part of the field, with an east-west orientation (fig. 5). Of the 227 identified eruptions in the Sierra Chichinautzin volcanic field, 157 have occurred in the last 35 k.y. In this group, the volcanic activity of the last 10 k.y. stands out with eruptions around 2 ka (Xitle and Chichinautzin volcanoes) and is localized to the central-western sector of the field (fig. 5). Jaimes-Viera and others (2018) noted that the northern part of the region contained an independent small grouping of volcanic vents, the Sierra de Santa Catarina. The Sierra de Santa Catarina is considered a separate volcanic field from

Table 1. Summary of the $^{40}Ar/^{39}Ar$ analyses of the selected samples in the Sierra Chichinautzin volcanic field carried out in this study.

[UTM, universal transverse Mercator; 14Q, zone 14; ka, kilo annum; ±, plus or minus; %, per cent; MSWD, mean square weighted deviates; Ar_i, initial argon]

Sample	North (UTM 14Q)	East (UTM 14Q)	Integrated age (ka)	Plateau age (ka)	Plateau information	Isochron age (ka)	Isochron information
El Elefante	509576	2133542	1,365±92	1,485±92	5 fractions 80% ^{39}Ar release MSWD = 0.59	1,876±311	5 fractions $^{40}Ar/^{36}Ar_i$ = 290±5 MSWD = 0.28
El Cantil	484293	2125179	1,516±21	1,537±17	4 fractions 93% ^{39}Ar release MSWD = 0.25	1,540±17	6 fractions $^{40}Ar/^{36}Ar_i$ = 294±75 MSWD = 0.22

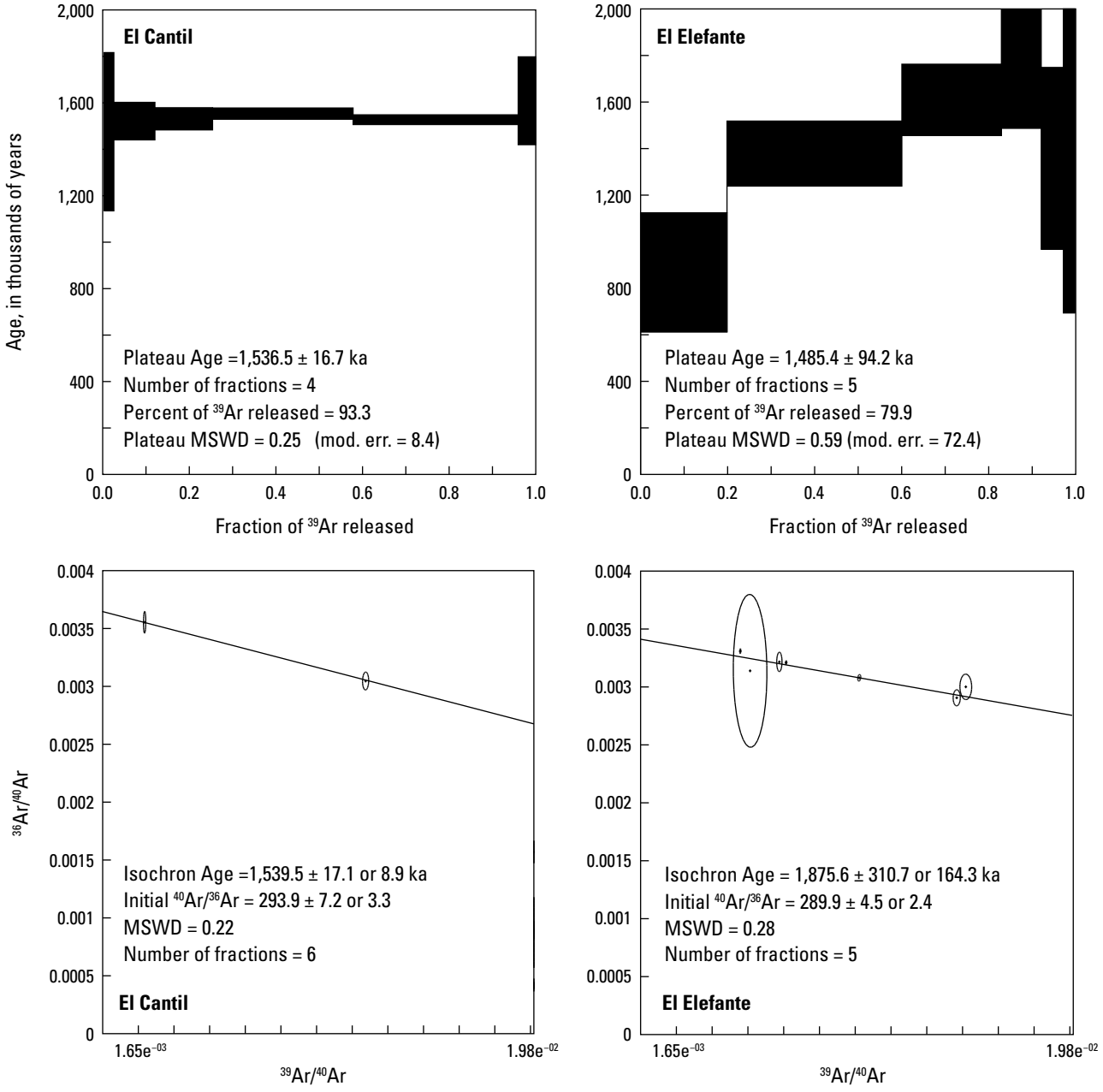

Figure 4. Graphs showing $^{40}Ar/^{39}Ar$ age spectra and isochron diagrams for samples from the El Cantil volcanic feature (left) and the El Elefante volcanic feature (right), which are monogenetic volcanoes within the Sierra Chichinautzin volcanic field. Ages are quoted at the 1-sigma level. MSWD, mean square weighted deviates. mod. err., model error.

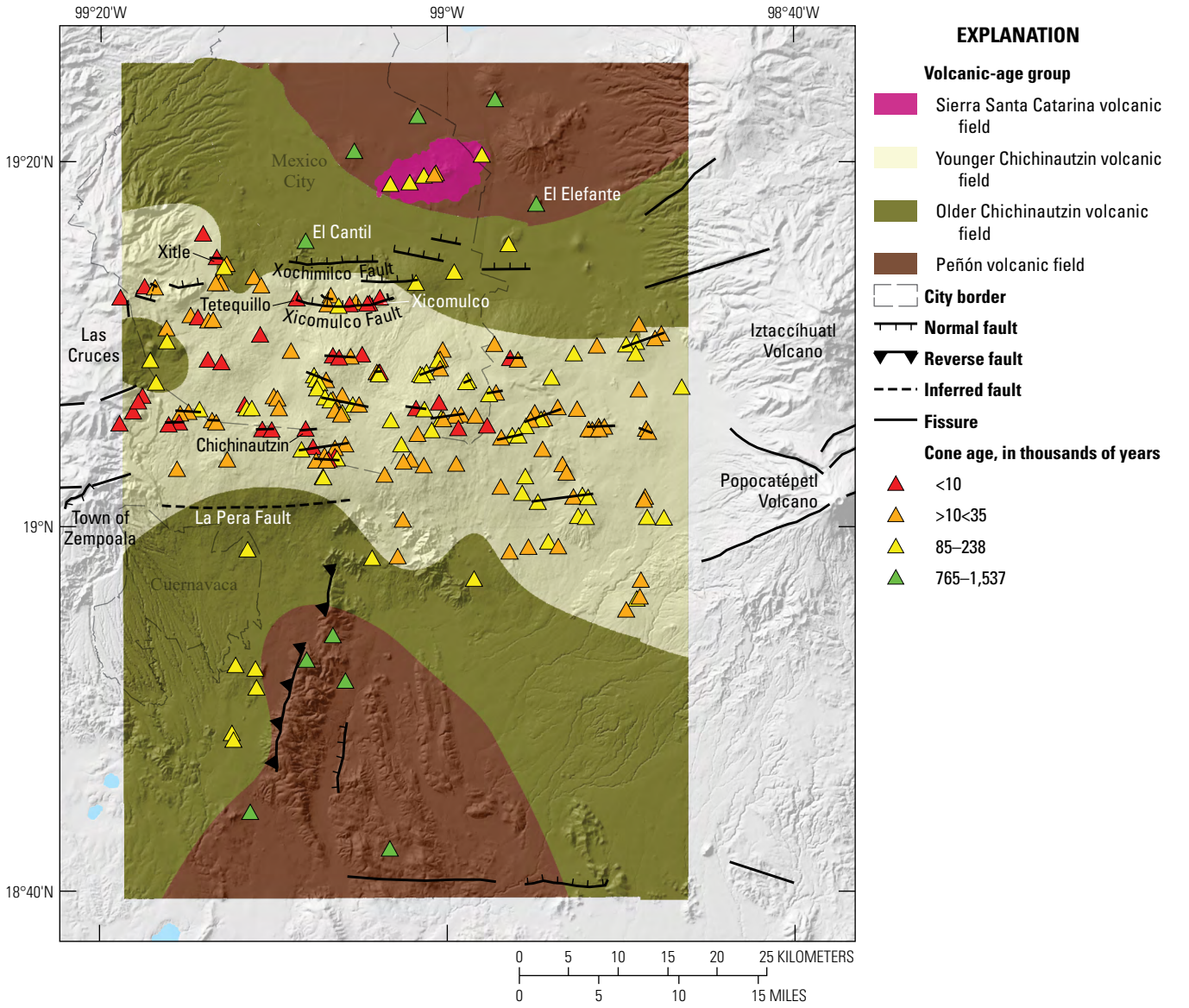

Figure 5. Map showing the ages of the eruptions within the Sierra Chichinautzin volcanic field, including the most recent ages from El Cantil volcano (1,537±17 thousand years ago) and El Elefante dome (1,485±92 thousand years ago). Modified from Jaimes-Viera and others, 2018.

the Sierra Chichinautzin volcanic field because it exhibits the highest values of zircon in the area, a different style of volcanism (phreatomagmatic, because of the presence of an ancient lake), and a completely different trend that is aligned northeast-southwest (Jaimes-Viera and others, 2018).

Seismic Activity in the Sierra Chichinautzin Volcanic Field

The UNAM-SSN seismic catalogue has recorded 841 seismic events in the Sierra Chichinautzin volcanic field area since 1973 (fig. 6; UNAM-SSN). The magnitude of the earthquakes ranges from 1 to 5. Most of these earthquakes are of shallow origin (<5 km depth) and associated with regional crustal faults. The deepest earthquakes, which are rare, have depths >31 km but <50 km. The distribution of epicenters forms two small groups. The first has magnitudes <2.6, shallow hypocenters (<5 km depth), and is located to the south of Mexico City. The second group is observed to the east of the Xochimilco and Xicomulco Faults, and many have magnitudes of 3.1–4. In general, these earthquakes are shallow, with depths <5 km, but some located at a greater depth of between 31 km and 50 km stand out. In the central and western parts of the field, where the most recent volcanoes are found, seismic activity is minimal, with magnitudes <4 and depths of 1–10 km (fig. 6). The spatial distribution of the hypocenters does not express any trend that could be associated with magma accumulation or migration.

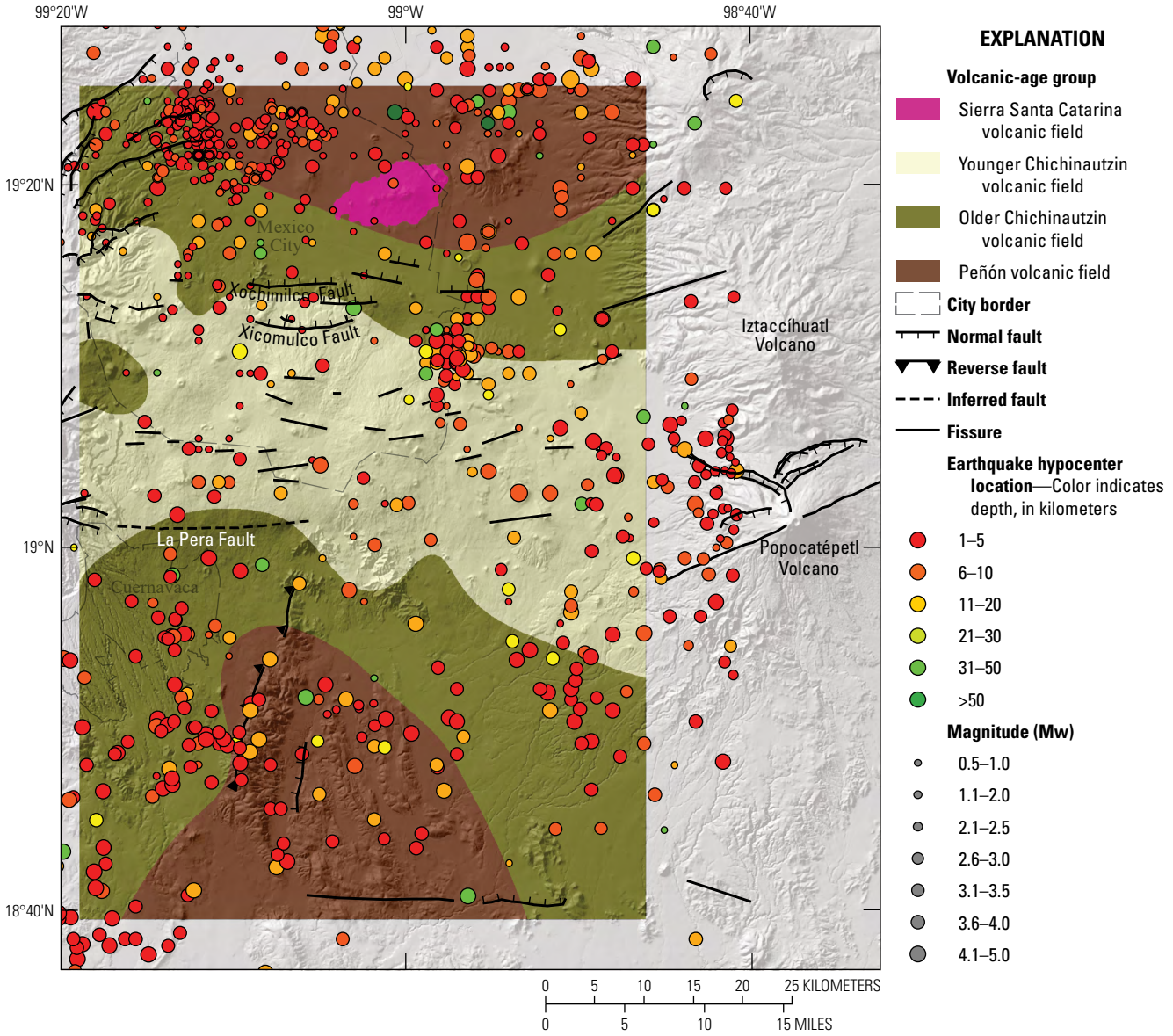

Figure 6. Map showing the seismic activity within the Sierra Chichinautzin volcanic field, with earthquakes colored by depth and scaled by magnitude. Each point corresponds to an individual seismic event. From the catalog of the Universidad Nacional Autónoma de Mexico Servicio Sismológico Nacional (UNAM-SSN). Modified from Jaimes-Viera and others, 2018.

State of the Plumbing System in the Sierra Chichinautzin Volcanic Field

The analysis of the elongation of the ellipsoid, derived from the eigenvectors of the vent-direction alignments (shape and azimuth) formed from the eruptions younger than 10 ka, permitted us to identify seven main feeder dike directions, five of which have a northwest-southeast trend and two have an east-west trend. The general trend (fig. 7) is parallel to the Middle America Trench (fig. 1).

Michoacán-Guanajuato Volcanic Field

In this section we will show how the data obtained, in the different analyses we have done, will allow us to describe the four volcanic fields that comprises the Michoacán-Guanajuato volcanic field, the distribution of the vents in each volcanic field, and the behavior of the volcanic activity through time and space.

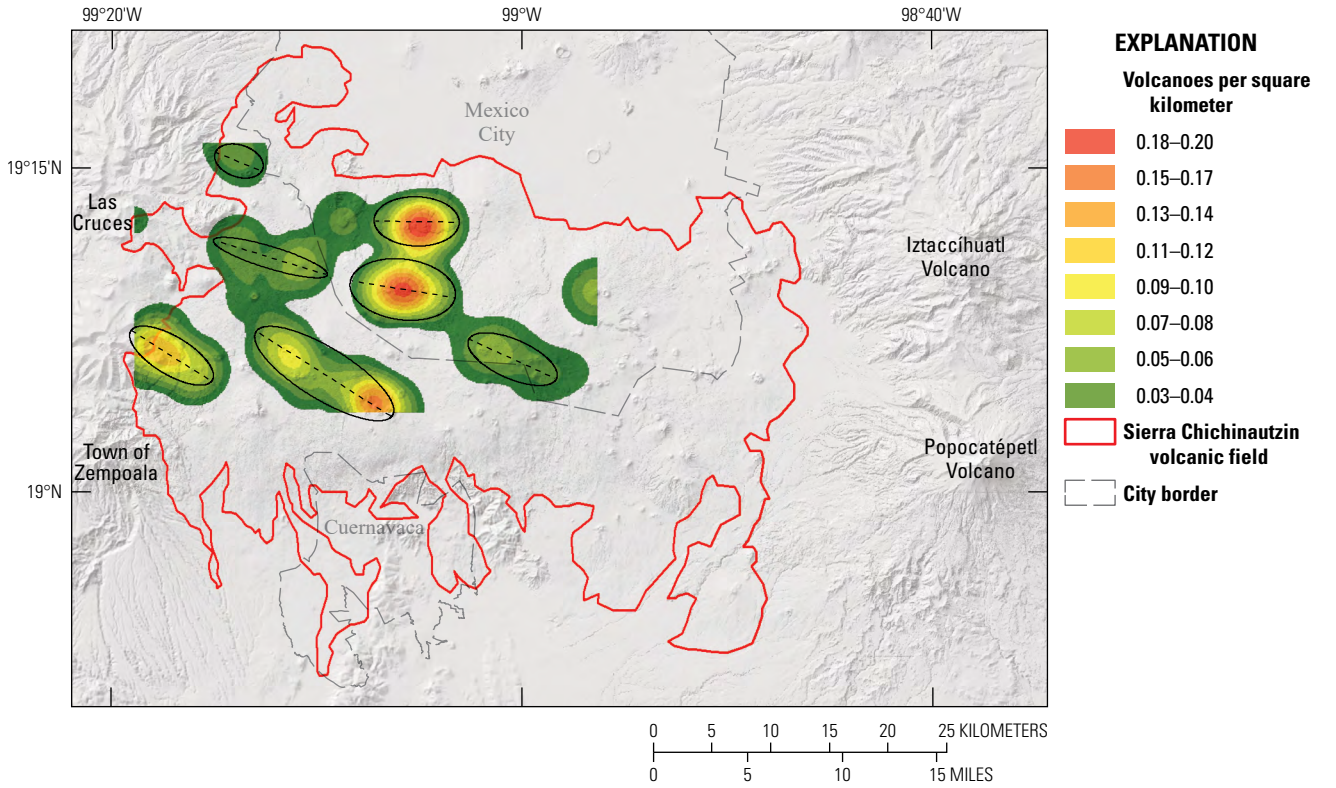

Figure 7. Map showing the position and trends of the feeder dikes in the Sierra Chichinautzin volcanic field based on vent-alignment analysis of the eruptions that are younger than 10,000 years old. Areas with less concentration of volcanoes per square kilometer than 0.02 have no color. The standard deviational ellipses, calculated from the respective eigenvectors Principal Components Analysis (PCA), are shown in black.

Kernel Density Analysis

The 15 km search radius used for the kernel analysis of the Michoacán-Guanajuato volcanic field produced groupings of at least four separate fields, making the Michoacán-Guanajuato a group of volcanic fields, or a superfield, with well-defined characteristics for each (fig. 8).

A total 1,148 volcanic vents in an area of 26,200 km^2, yielded an average concentration of 0.043 vents/km^2 for the whole volcanic field. In addition to the analysis of volcano concentration, the geomorphological characteristics of the cones of the Michoacán-Guanajuato volcanic field were considered to identify the four clusters that comprise it (supplementary table 2). The first cluster, which we named Valle de Santiago volcanic field, is located in the northeastern part of the Michoacán-Guanajuato volcanic field. The Valle de Santiago volcanic field is controlled by the active La Alberca-Teremendo Fault system (Pasquarè and others, 1991; Ferrari and others, 1994; Kurokawa and others, 1995; Soria-Caballero and others, 2019), which has a northeast-southwest trend. We found 187 vents in the Valle de Santiago volcanic field in an area of 7,294 km^2, which yields a density of 0.025 vents/km^2. In this field, the maximum concentration value of volcanoes is lower than in the rest of the Michoacán-Guanajuato volcanic field (<0.1 vents/km^2), and maars are very common.

We named the second cluster the Uruapan volcanic field, and it is controlled by the Cotija Fault and Chapala Fault systems (Kurokawa and others, 1995; Ferrari and others, 1994; Pasquarè and others, 1991). Cotija Fault system has a northwest-southeast trend, whereas Chapala Fault system has an east-west trend. In the north part of the Uruapan volcanic field, the Penjamillo graben (Kurokawa and others, 1995; Ferrari and others, 1994; Pasquarè and others, 1991) represents the border with the Valle de Santiago volcanic field (fig. 8). In the Uruapan volcanic field, there are 448 vents distributed across an area of 10,100 km^2, giving a concentration of 0.044 vents/km^2. The maximum concentration of vents is <0.15 vents/km^2. Within this field, the eruption of Parícutin volcano took place during the years of 1943–1952, which is the most recent eruption within the Michoacán-Guanajuato volcanic field. Other recent eruptions (<1 ka) in the Uruapan volcanic field are those of the Metate and Prieto volcanoes (Chevrel and others, 2016; Reyes-Guzmán, and others, 2023).

The third cluster, here named Apatzingán volcanic field, is south of the Uruapan volcanic field and shares the locally known volcanic feature Tancítaro volcano along the Uruapan's south border. Volcanoes within Apatzingán volcanic field are aligned following a northeast-southwest trend, contrasting with the Cotija Fault system and Chapala Fault system trend of the northern neighbor Uruapan volcanic field (fig. 8). We counted

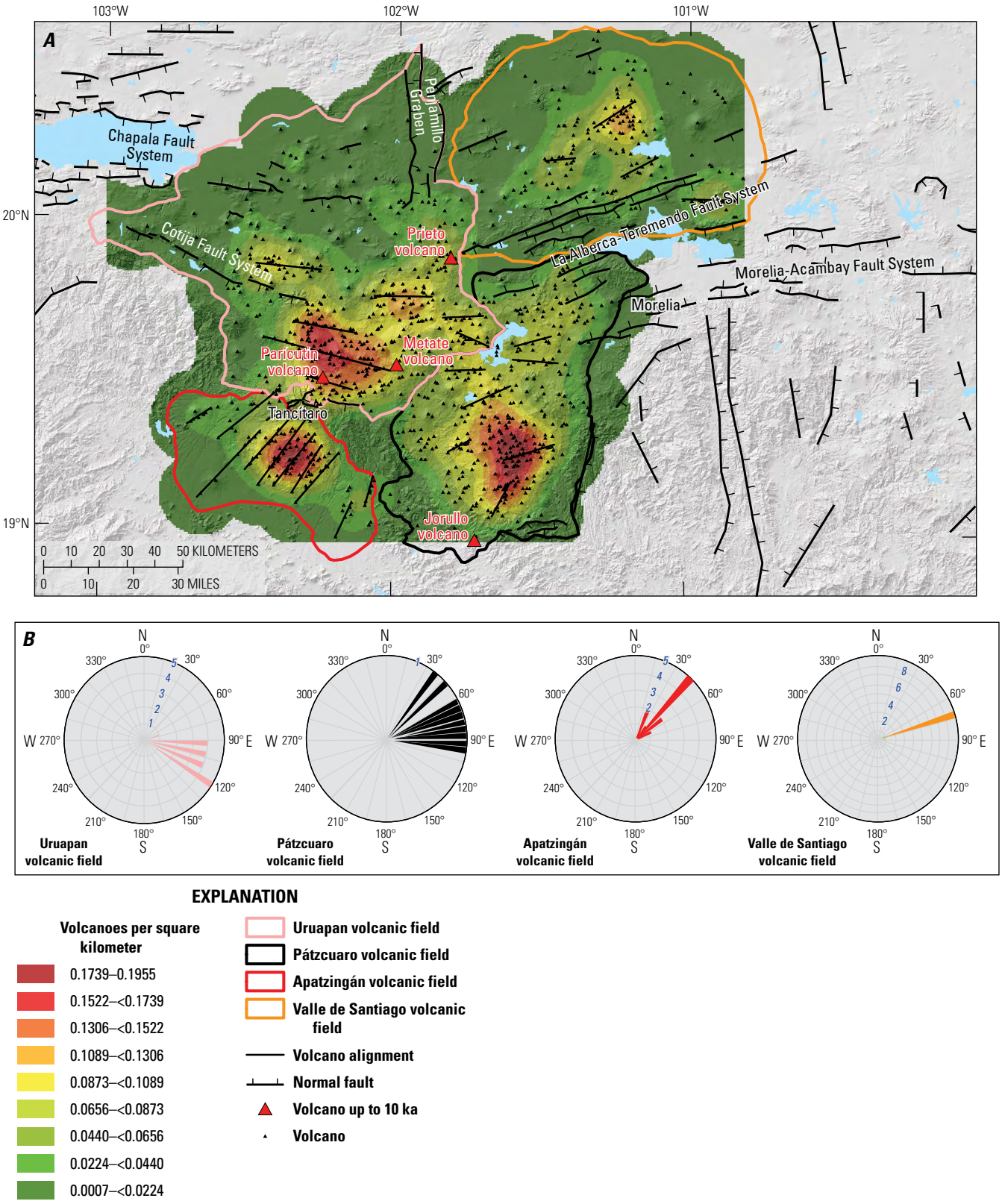

Figure 8. Map and rose diagrams showing the results from kernel density analysis of the Michoacán-Guanajuato volcanic field. *A*, Map of the kernel density results of the Michoacán-Guanajuato volcanic field, divided into the four smaller volcanic fields (Uruapan volcanic field, Pátzcuaro volcanic field, Apatzingán volcanic field and Valle de Santiago volcanic field). *B*, Rose diagrams for the fault azimuthal trend direction for the four fields. Numbers in blue indicate the number of faults or fissures in that direction.

143 vents in the Apatzingán volcanic field within an area of 2,767 km^2, which yields a concentration of 0.051 vents/km^2. In the Apatzingán volcanic field, the maximum concentration of vents is 0.17 vents/km^2.

We named the fourth cluster, located in the southwest part of the Michoacán-Guanajuato volcanic field, the Pátzcuaro volcanic field. The Pátzcuaro volcanic field is controlled in its northern part by the Morelia-Acambay Fault system (Kurokawa and others, 1995; Ferrari and others, 1994 Pasquarè and others, 1991), which has a northeast-southwest trend. There are 370 vents in an area of 6,048 km^2, which yields a concentration of 0.061 vents/km^2—the maximum concentration of the four volcanic fields of the Michoacán-Guanajuato volcanic field. It is also the location with the highest maximum concentration of vents (0.195 vents/km^2). The 1759–1774 eruption of Jorullo volcano extended the southern edge of the Pátzcuaro volcanic field, being the southernmost volcano of the Michoacán-Guanajuato volcanic field (fig. 8*A*). Fault, fissure, and vent alignments in each volcanic field vary slightly from 90 degrees to 120 degrees in the Uruapan volcanic field, 40 degrees to 100 degrees in the Pátzcuaro volcanic field, between 20 degrees and 60 degrees in the Apatzingán volcanic field, and the trend in the Valle de Santiago volcanic field is about 70 degrees (fig. 8*B*).

Vent Cluster Agglomerative Hierarchical Dendrogram Analysis

The appropriate number of clusters for each volcanic field was obtained by analyzing the agglomerative hierarchical dendrogram (fig. 9). This dendrogram represents each vent assigned to a proper cluster characterized by the average distance of all the vents within the cluster from the centroid and the location of the centroid, assigning it a similarity value that decreases with distance, or, in other words, a dissimilarity value that increases with distance. The smaller the distance is between the compared vents, the greater their similarity. Figure 9 shows that the volcanoes in Michoacán-Guanajuato

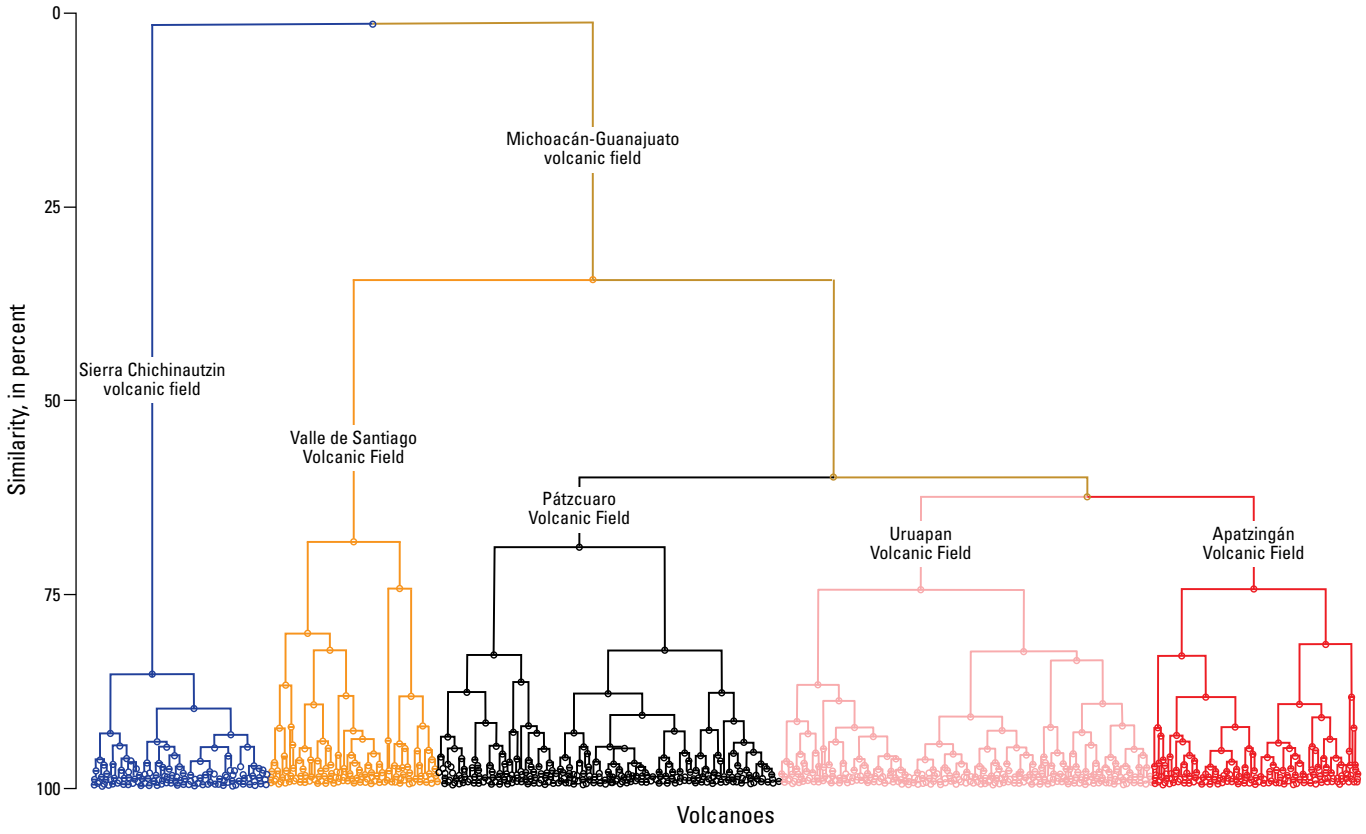

Figure 9. Dendrogram representing the grouping of volcanoes into one cluster within the Sierra Chichinautzin volcanic field, and the four clusters that make up the Michoacán-Guanajuato volcanic field.

and Sierra Chichinautzin volcanic fields are 0 percent similar, due the distance between both volcanic fields. However, Valle de Santiago volcanic field shares about 30 percent of similarity with the other three clusters in the Michoacán-Guanajuato volcanic field, whereas this percentage increases to 60 percent among the Uruapan, Apatzingán, and Pátzcuaro volcanic fields (fig. 9). These results are like those obtained in the kernel density analysis (fig. 8).

Cone Morphometry and Age Estimation

The *h/wb* ratio was used to determine the degree of scoria cone erosion over time (see supplementary table 2). Assuming the scoria cones are bedded and unwelded, low values were associated with more eroded scoria cones (fig. 10), which means that the scoria cones have been exposed to the environment for more time, whereas higher values mean that the scoria cones are less eroded, having been exposed for less time. According to the rate of erosion of the cones, the Valle de Santiago volcanic field has *h/wb* ratios between 0.01 and 0.17; the Apatzingán volcanic field between 0.02 and .23; the Pátzcuaro volcanic field between 0.03 and 0.26; the Uruapan volcanic field between 0.03 and 0.27; and the Sierra Chichinautzin volcanic field between 0.04 and 0.27 (see supplementary table 2). Corresponding with these data, the cones of the Valle de Santiago volcanic field are predominantly older, and it is not possible to find cones with young morphology. In the Apatzingán volcanic field, cones with young features predominate, and cones with older morphology are scarce. In the Pátzcuaro volcanic field, cones with dissected morphology predominate and, although they are infrequent, it is also possible to observe cones with younger morphology. Cones of the Uruapan volcanic field have a bimodal morphology with both relatively old and poorly preserved cones alongside relatively young and well-preserved cones. In contrast, in the Sierra Chichinautzin volcanic field, the cones are predominantly young (fig. 10).

The distribution of the cones in the Michoacán-Guanajuato volcanic field (fig. 11) shows that the cones with older morphology are mainly located in the northern part of the volcanic field, and it is observed that the younger morphologies are concentrated in the central-southwest part, which matches the histograms from the Michoacán-Guanajuato volcanic field.

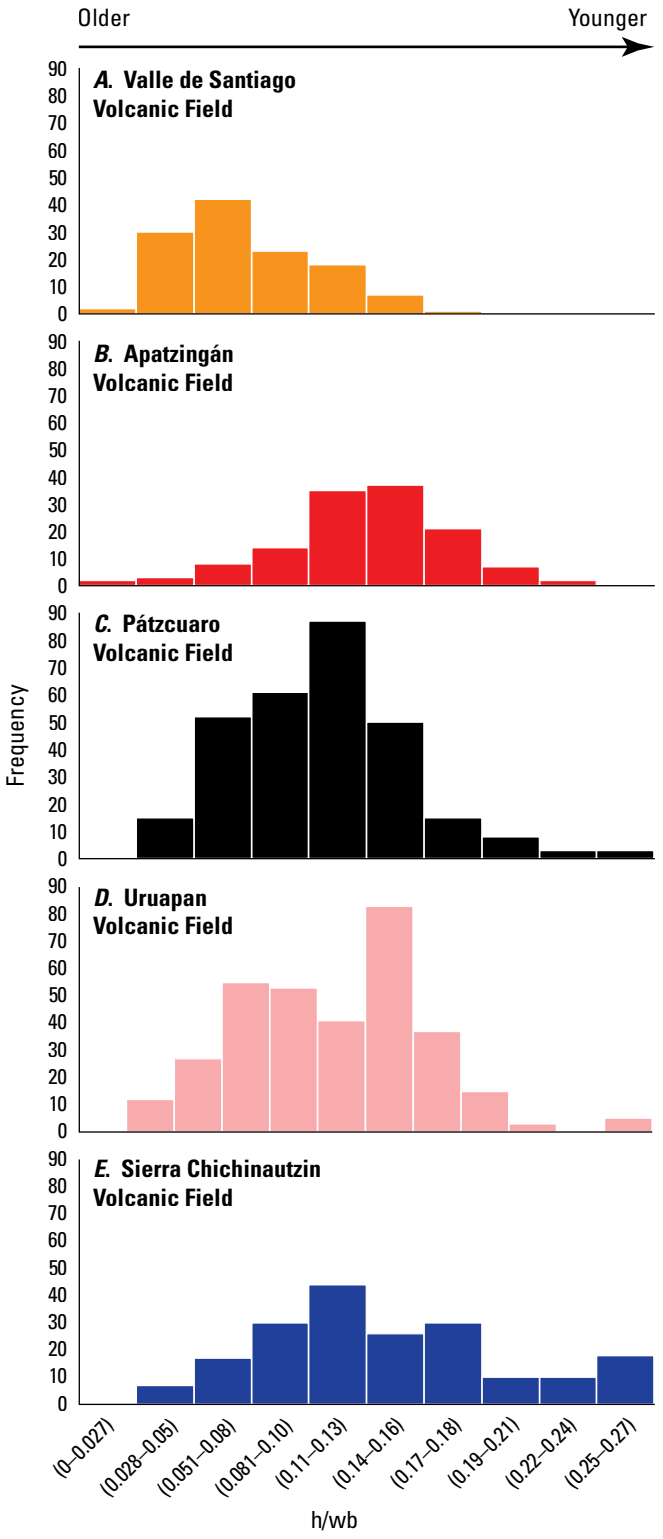

Figure 10. Histograms showing the distribution of the morphology (height over base diameter [*h/wb*]) of the Valle de Santiago (*A*), Apatzingán (*B*), Pátzcuaro (*C*), Uruapan (*D*), and Sierra Chichinautzin (*E*) volcanic fields. The lower the *h/wb* ratio, the older the cone, whereas higher ratios indicate younger cones.

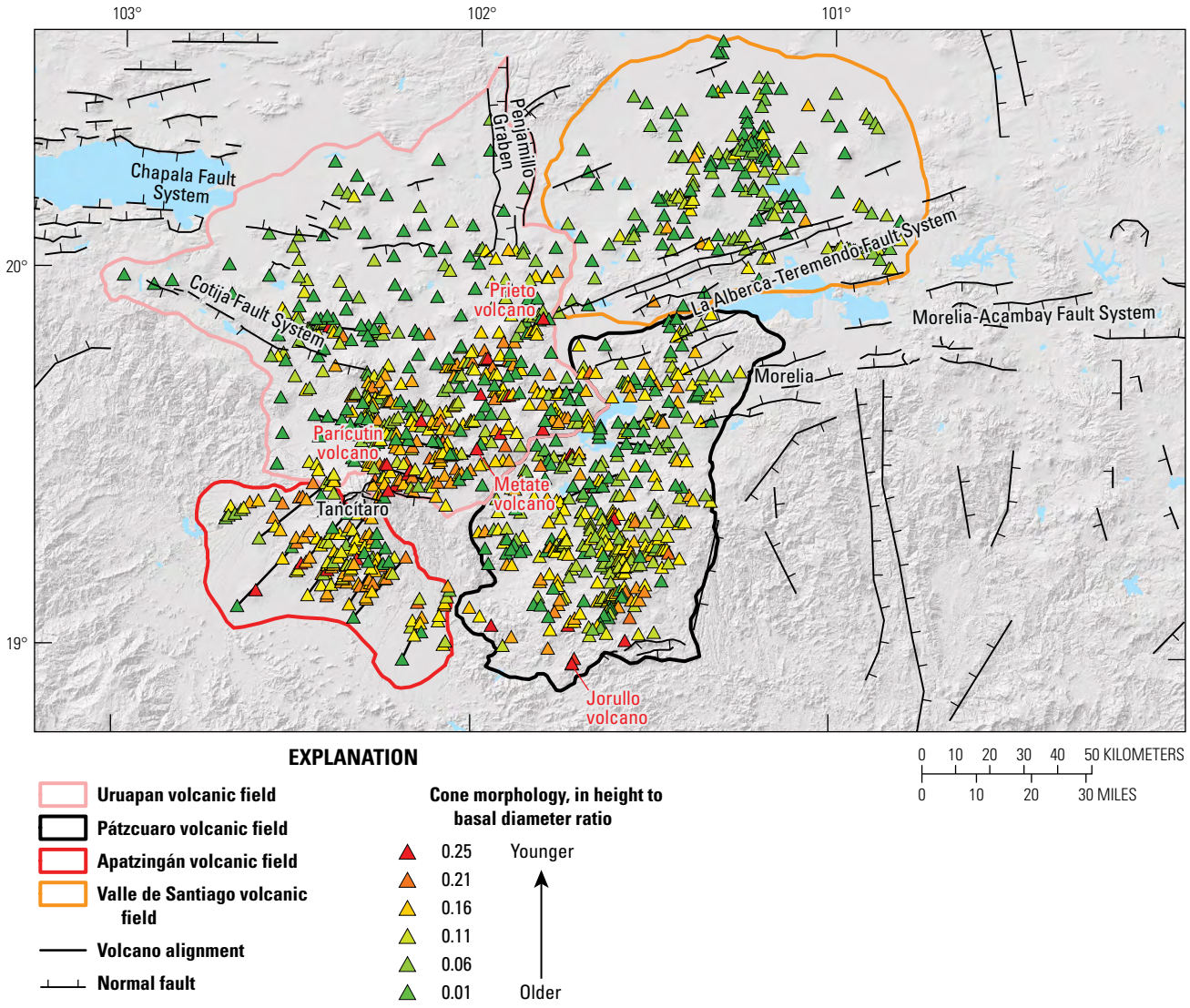

Figure 11. Map of the cone morphology in height to basal diameter ratio within the Michoacán-Guanajuato volcanic field, showing the location of the old and young cones.

Seismic Activity in the Michoacán-Guanajuato Volcanic Field

The analysis of 9,016 earthquakes in the Michoacán-Guanajuato volcanic field since 1973 shows that seismic activity is concentrated in the region around Parícutin Volcano, at the south edge of the Uruapan volcanic field, clearly delimited by the Tancítaro volcano (fig. 12). Seismic swarms have occurred between the Tancítaro and Parícutin volcanoes in 1997, 1999, 2000, 2006, 2020, 2021 (Legrand and others, 2023), 2022, and 2023. The deepest earthquakes in this area are 31–50 km, but the most common depth is <10 km. Nevertheless, in the most recent swarms in 2022 and 2023, the depths became shallower compared to the swarms of previous years, getting to be <5 km. It is possible to observe a trend of earthquakes toward the surface from east (from Metate and Uruapan volcanoes) to west (to Parícutin volcano) (fig. 12). The maximum magnitude registered in this area is <5, and the most common magnitude is <3. Seismic activity elsewhere within the Michoacán-Guanajuato volcanic field is scarce. Subduction-related seismic activity (>50 km depth) is seen and is limited to the southern edge of the Apatzingán volcanic field (fig. 12).

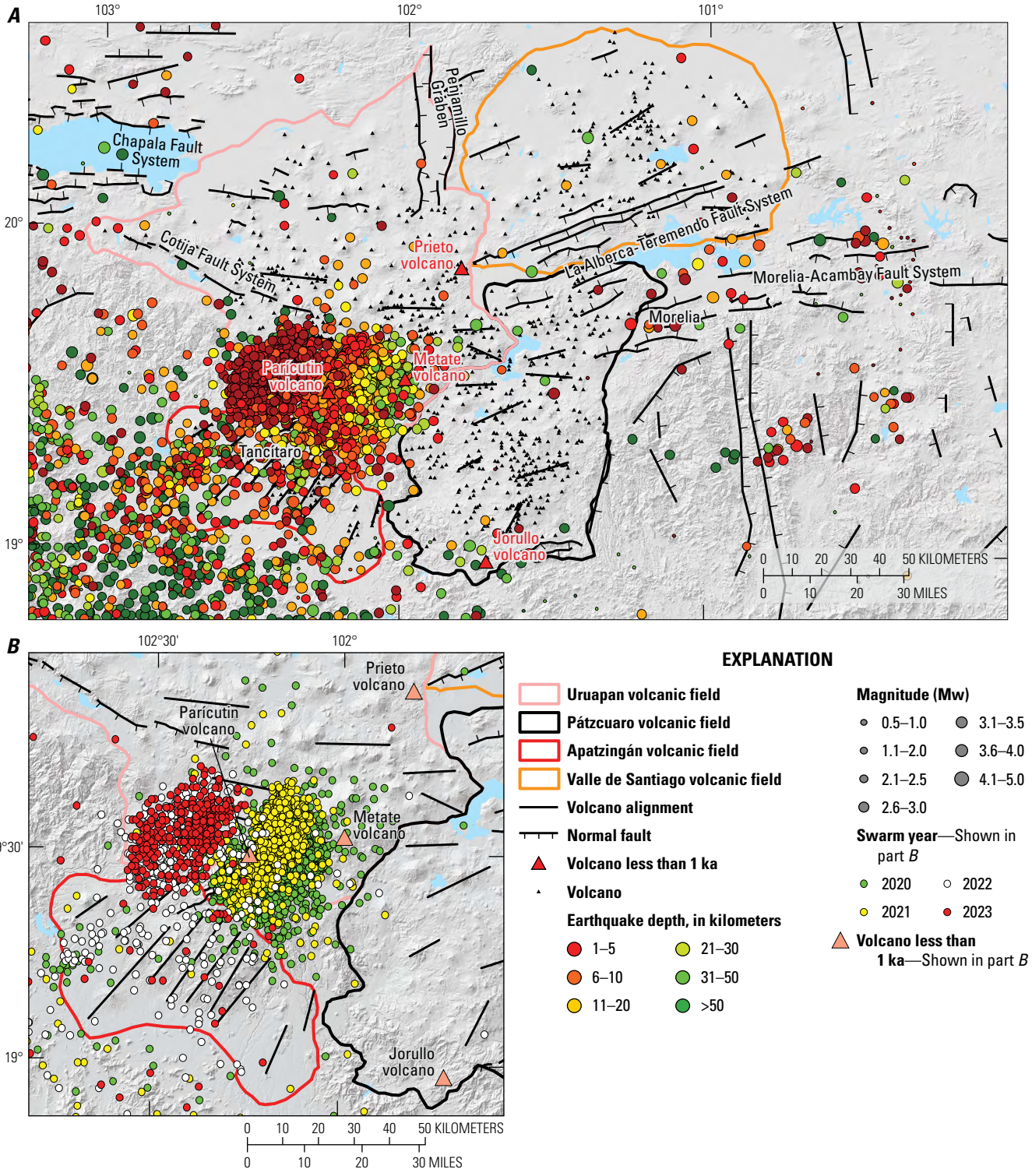

Figure 12. Maps showing seismic activity in the Michoacán-Guanajuato volcanic field. *A*, Map of seismic activity from 1973 to 2023 within the Michoacán-Guanajuato volcanic field, with earthquakes colored by depth and scaled by magnitude. Each point represents an individual seismic event. Data are from the catalog of the Universidad Nacional Autónoma de Mexico Servicio Sismológico Nacional (UNAM-SSN, 2023). *B*, Inset map of southern Uruapan, western Pátzcuaro, and northern Apatzingán volcanic fields showing seismic swarms from 2020 to 2023, colored by year.

Discussion

Density and Agglomerative Hierarchical Dendrogram Analysis

The Sierra Chichinautzin volcanic field has 227 volcanoes and an approximate area of ~3,500 km^2. The volcanoes are mostly andesitic but consist of some basaltic and dacitic rock. According to the ages obtained here and previous data (Jaimes-Viera and others, 2018), this volcanic field started its activity ~1.5 Ma. The Michoacán-Guanajuato volcanic field has 1,148 volcanoes that occur over an area of 26,200 km^2. Activity in this field began around 5 Ma (Hasenaka and Carmichael, 1985a, 1985b; Ban and others, 1992) and has mainly resulted in basaltic cinder cones and maars. If we divide the number of volcanoes in Sierra Chichinautzin volcanic field and in Michoacán-Guanajuato volcanic field by their respective total areas, we found that the density of volcanoes is higher in the Sierra Chichinautzin volcanic field (0.064 vents/km^2) than in the Michoacán-Guanajuato volcanic field (0.043 vents/km^2).

The machine learning, agglomerative clustering approach, however, demonstrates that the Michoacán-Guanajuato volcanic field consists of four distinct volcanic fields. In this sense, as we proposed before, the Michoacán-Guanajuato volcanic field is a "superfield," and it is appropriate to consider the vent density within each of the four volcanic fields within it separately. When we treat each of the different volcanic fields that make up the Michoacán-Guanajuato volcanic field independently, we find that the density for the Valle de Santiago volcanic field is 0.025 vents/km^2, 0.044 vents/km^2 in the Uruapan volcanic field, 0.051 vents/km^2 in the Apatzingán volcanic field, and 0.061 vents/km^2 in the Pátzcuaro volcanic field. Despite analyzing each volcanic field of the Michoacán-Guanajuato volcanic field separately, the highest density of volcanoes is still in the Sierra Chichinautzin volcanic field, and the Pátzcuaro volcanic field is comparable.

A similar trend of behavior to the density analysis is also seen with the search radius for the kernel analysis, defined by the distance of the most isolated volcano to its nearest neighbor in each field. In the Sierra Chichinautzin volcanic field, the search radius used was 9 km, whereas in the Michoacán-Guanajuato volcanic field, 15 km was used. The agglomerative hierarchical dendrogram (fig. 9) confirmed the subdivision of the Michoacán-Guanajuato volcanic field into four different volcanic fields because there are significant differences in the average distance of all the vents within a cluster from the centroid. The similarity among volcanic fields within the Michoacán-Guanajuato volcanic field is about 30 percent for the Valle de Santiago volcanic field and 60 percent for the rest of the volcanic fields.

The distribution of most of the volcanoes in the Sierra Chichinautzin volcanic field is concentrated in the central part of the field, forming a main cluster with an east-west orientation (figs. 3 and 5), corresponding to the trend of La Pera Fault (Norini and others, 2006) and Xochimilco and Xicomulco Faults (Campos-Enríquez and others, 2015). In this area, the highest concentration of volcanoes is 0.278 vents/km^2, whereas the highest concentration of volcanoes in the Michoacán-Guanajuato volcanic field is found in the Pátzcuaro volcanic field, with 0.195 vents/km^2.

The four volcanic fields that make up the Michoacán-Guanajuato volcanic field are also controlled by the general trend of the regional faulting. Importantly, the numbers of vent alignments and their orientations vary between the four volcanic fields of the Michoacán-Guanajuato volcanic field. Similarly, the faults systems associated with these four volcanic fields have different trends (figs. 8 and 11). The Valle de Santiago volcanic field is controlled by La Alberca-Teremendo Fault system, and the Uruapan volcanic field is controlled by the Cotija Fault system and the Chapala Fault system, with the Penjamillo graben forming the border between the Uruapan volcanic field and the Valle de Santiago volcanic field. Tancítaro volcano is the border of the Uruapan volcanic field with the Apatzingán volcanic field. Volcanoes in the Apatzingán volcanic field are aligned along northeast-southwest trends. The Pátzcuaro volcanic field is controlled by the Morelia-Acambay Fault System. The Apatzingán volcanic field, which is closest to the trench, is dominated by vent alignments that are parallel to the direction of plate convergence. Farther from the trench, arc-parallel vent alignment and faults systems predominate. In other words, it is important to distinguish the volcanic fields within the Michoacán-Guanajuato volcanic field to identify and understand changes in volcano-tectonic setting across the Michoacán-Guanajuato volcanic field.

Geochronology and Spatial Distribution of Ages

In the Michoacán-Guanajuato volcanic field, monogenetic volcanism extends from 5 Ma to the present, with at least 1,148 eruptions, whereas the volcanism in the Sierra Chichinautzin volcanic field began ~1.5 Ma, with at least 227 eruptions. Most of the eruptions in the Sierra Chichinautzin volcanic field (157) have occurred in the last 35 k.y. Although there is this difference between the onset of volcanism in each volcanic field, it can be observed that, though the most recent recorded eruptions have occurred in the Michoacán-Guanajuato volcanic field (Jorullo volcano (1759–1744) and Parícutin volcano(1943–1952)), the eruptive recurrence rate is twenty times higher in the Sierra Chichinautzin volcanic field (0.0044 eruptions/year) than in the Michoacán-Guanajuato volcanic field (0.00022 eruptions/year). Recent eruptions in the Sierra Chichinautzin volcanic field (<10 ka) are in the central and western parts of the field, whereas in the Michoacán-Guanajuato volcanic field recent eruptions (<1 ka) are in the southeastern part of the Uruapan volcanic field and the southern parts of the Apatzingán and Pátzcuaro volcanic fields. In the northern part of the Uruapan volcanic field and in the whole Valle de Santiago volcanic field, only oldest eruptions can be found, with relative ages determined from the degree of cone erosion, which is consistent with the ages (~5 Ma) proposed by Murphy (1986).

Many authors have noted that alignments of vents following the trend of the major faults systems are common (Williams, 1956; Connor, 1987; 1990; Hasenaka and Carmichael, 1985a, 1985b). Ban and others (1992) found that northern volcanoes, such as those of the Valle de Santiago volcanic field and the northern part of the Uruapan volcanic field, are older than the southern volcanoes of the Pátzcuaro and Apatzingán volcanic fields (around the Tancítaro volcano area) and in the southeastern part of the Uruapan volcanic field. According to Hasenaka and others (1994), volcanism in the Michoacán-Guanajuato volcanic field began showing a clear migration trend toward the southwest at 3 Ma. Connor (1990) and Mazzarini and others (2010) also subdivide the Michoacán-Guanajuato volcanic field into four different zones through a kernel vent clusters analysis. Furthermore, Di Traglia and others (2014) also found that the southernmost part of the Michoacán-Guanajuato volcanic field is composed of two different clusters. This is consistent with what we found for this field. Moreover, Connor (1990) concluded that in the three southern volcanic fields of the Michoacán-Guanajuato volcanic field (the Uruapan volcanic field, Apatzingán volcanic field, and Pátzcuaro volcanic field) there are only high-magnesium lavas, indicating that magma transport is significantly enhanced in this area, associated with northeast-southwest alignments. In the southern part of the Michoacán-Guanajuato volcanic field, around Tancítaro, a greater concentration of scoria cones with ages <1.2 Ma can be found, which is similar to the age of early volcanism observed in the Sierra Chichinautzin volcanic field. The historical eruptions of Jorullo and Parícutin volcanoes took place in the southern Michoacán-Guanajuato volcanic field (Ban and others, 1992; Pioli and others, 2008; Ownby and others, 2011). Thus, age, and perhaps geochemistry, like relationship to faults, is best understood in terms of the four volcanic fields within the whole Michoacán-Guanajuato volcanic field.

In the Sierra Chichinautzin volcanic field, the ages of the eruptions are well constrained, which allowed the construction of a spatial distribution model of the eruptions over time. Volcanism began in the northern part of the field (fig. 5), with the eruption of the El Cantil volcano (1,537±17 ka) followed by the eruption of the El Elefante volcano (1,485±92 ka). These ages are consistent with the start of the volcanic activity in the Sierra Chichinautzin volcanic field that was found by Jaimes-Viera and others (2018). Volcanism of similar age is also found in the southern part of the Sierra Chichinautzin volcanic field. These first-stage cones are widely spaced and form a northeast-southwest alignment. A second stage of volcanism occurred during 238–85 ka and is found in the central part and towards the edges of the field and also has a northeast-southwest trend (fig. 5). After a temporal gap of almost 60 k.y., a third stage of volcanism resumed ~35 ka only in the central part of the field and with alignments following an east to west trend (fig. 5). This volcanism has remained active through the present and has produced the largest number of volcanoes: 157 of the 227 identified in the Sierra Chichinautzin volcanic field. There exists the possibility that old vents could have been buried by the newer erupted lavas, which would increase the total number of volcanoes in the Sierra Chichinautzin volcanic field. Volcanism of the last 10 k.y. in the Sierra Chichinautzin volcanic field (fig. 5) can only be found in the central-western sector of the central part of the field and has a clear east-west trend (fig. 5). Jaimes-Viera and others (2018) described a fourth stage of volcanic activity in the Sierra de Santa Catarina (132±70 to 23±4 ka; fig. 5), that is distinct from the rest of the volcanoes of the Sierra Chichinautzin volcanic field due the high zircon content, a completely different trend (northeast-southwest), and phreatomagmatic activity.

The alignments of the cones in the Sierra Chichinautzin volcanic field exhibit a progressive change from north-northeast-south-southwest to northeast-southwest to east-west through time; these changes are probably associated with variations in the stress field in the region. The rotation of the stress fields in a clockwise direction seems to control the distribution of the volcanic fields, in which the north-south extension increases with time, allowing the east-west alignment of cones to dominate, as described by Jaimes-Viera and others (2018).

Seismic Activity

Seismicity in Sierra Chichinautzin Volcanic Field

The analysis of 841 seismic events in the Sierra Chichinautzin recorded since 1973 has shown no trend that could be associated with any shallow movement of magma. In general, seismic activity within the Sierra Chichinautzin volcanic field is minimal, with magnitudes <4 and depths of 1–10 km. Two main groups of earthquakes are evident, the first being located within the southern part of Mexico City. The earthquakes in this region have been associated with regional tension because of the subsidence of Mexico City into lacustrine sediments of the Basin of México (UNAM-SSN, 2023), which can act as a triggering mechanism (Havskov, 1982). It has also been hypothesized that large earthquakes generated at the coast could give rise to unbalanced conditions that reactivate old faults and trigger local earthquakes—this could be associated with a fluid movement induced by strain that can cause shallow earthquakes at about 2 to 4 km in depth (Singh and others, 1998). The second group of earthquakes in the Sierra Chichinautzin volcanic field is located on the western part of the Xochimilco and Xicomulco Faults. According to Campos-Enríquez and others (2015), the focal mechanism of earthquakes corresponds well with the Xicomulco Fault; therefore, these earthquakes are most likely associated with slip on this fault.

Seismicity in the Michoacán-Guanajuato Volcanic Field

The analysis of 9,016 earthquakes since 1973 has shown that the seismic activity within the Michoacán-Guanajuato volcanic field is concentrated in the region between Parícutin and Tancítaro volcanoes in the southern part of the Uruapan volcanic field. Seismic activity elsewhere within the Michoacán-Guanajuato volcanic field is less common. In the region where earthquakes are concentrated, a trend of earthquakes is observed toward the surface, with variations in depth, from east to west. The deepest earthquakes in this area are at 31–50 km, but the most common

depth is <10 km, reaching <5 km during swarms in 2022 and 2023. Legrand and others (2023) note that these swarms have been associated with repeated movements of magma toward the surface, which indicates that magma has stalled at shallow levels during ascent from the mantle. During future unrest, it is possible that this magma could make it to the surface.

State of the Plumbing System in the Sierra Chichinautzin Volcanic Field

Feeder dikes are expressed at the Earth's surface by alignments of volcanic vents (Connor and others, 1992; Paulsen and Wilson, 2010; Rooney and others, 2011; Muirhead and others, 2015; Mazzarini and others, 2016). Through the azimuth of the maximum axis of the standard deviational ellipse we identified seven feeder dikes for >20 eruptions that occurred in the last <10 ka in the Sierra Chichinautzin volcanic field, with a general southeast-northwest trend. The trend of the feeder dikes is a result of the combination of the magma overpressure, the differential stress field, and weaknesses in the host rock (Takada, 1994; Jolly and Sanderson, 1997; Connor and Conway, 2000; Le Corvec and others, 2013). The areas in which these feeder dikes are located coincide with the areas with the highest probability of hosting a future eruption identified by Nieto-Torres and Martin Del Pozzo (2019) and Nieto-Torres and others (2023). The last eruptions within the Sierra Chichinautzin volcanic field took place 1600-2000 years ago at Chichinauztin and Xitle volcanoes (Nieto-Torres and others, 2023; Blanco and Guilbaud, 2025). No evidence of recent changes in the stress field have been found in the Sierra Chichinautzin volcanic field, so it is likely that a future eruption will be fed by dikes with similar orientations.

Preparing for an Eruption

Preparing for an eruption within the Uruapan volcanic field, which is considered to be the most likely area of future eruptive activity based on geological history and seismicity, may be aided by strengthening monitoring systems and reinforcing measures to deal with volcanic hazards and risk. An eruption and its effects can last for a decade or more, as evident from eruptions of Jorullo and Parícutin volcanoes, and social and political systems may not be prepared to deal with a situation of such magnitude. In the Sierra Chichinautzin volcanic field, a complete evaluation of volcanic risk was recently done, in which the cost and effects of an eruption were estimated (Nieto-Torres and others, 2023). A similar evaluation could also be done for the Uruapan volcanic field. This evaluation could include both direct (damage to buildings and properties) and indirect (loss of business, costs of evacuation, relocation) consequences of an eruption, as well as the costs associated with clean-up of tephra. A similar assessment was done in the Auckland volcanic field in New Zealand (Paton and others, 1999). The design of evacuation routes and shelters could be addressed by such an evaluation, which could also include ongoing exercises with the population and civil protection to ensure awareness of volcanic hazards, and possibly even assessments related to the construction of barriers to protect infrastructure as done in Iceland during the 2021 Geldingadalir eruption (Sigtryggsdóttir and others, 2025).

Conclusions

We determined that the Michoacán-Guanajuato volcanic field, considered one of the largest concentrations of volcanoes on Earth, is not a single volcanic field as it has been considered in past studies. Rather, four main volcanic fields were identified within the Michoacán-Guanajuato volcanic field and are controlled by different fault systems. Here we propose to name these fields the Valle de Santiago volcanic field, the Uruapan volcanic field, the Apatzingán volcanic field, and the Pátzcuaro volcanic field, after the main cities within each field. Recognition of these four volcanic fields makes it easier to interpret the volcanotectonic setting, variations in geochemistry, and ages among and within the different volcanic fields.

Although there is a greater number of volcanoes in the Michoacán-Guanajuato volcanic field, they are distributed over an area seven times larger than the volcanoes in the Sierra Chichinautzin volcanic field, so the concentration of volcanoes is greater in the Sierra Chichinautzin volcanic field—0.064 vents per square kilometer (vents/km^2) versus 0.043 vents/km^2 in the Michoacán-Guanajuato volcanic field. Furthermore, the maximum concentration of volcanoes observed within each field is also higher in the Sierra Chichinautzin volcanic field—0.278 vents/km^2 versus 0.195 vents/km^2 in the Michoacán-Guanajuato volcanic field.

In the Sierra Chichinautzin volcanic field, the most recent eruptions were located in the central and western part of the field; however, there is no seismic evidence, or evidence of any other kind, for subsurface magmatic activity in the region. On the other hand, in the Uruapan volcanic field, recent shallow seismic swarms and their location near Parícutin volcano, where the most recent eruption in the area took place, suggest that this area could be a location of future eruptive activity.

Effective monitoring could make it possible to detect the precursors of volcanic activity in a timely manner, and our analysis notes that the Uruapan volcanic field and Sierra Chichinautzin volcanic field are especially important targets for any expanded monitoring capabilities. Campaigns to heighten awareness of volcanic hazards in the public could help local residents prepare for any future volcanic activity that may occur.

Acknowledgments

Carmen Jaimes Viera gives thanks to Secretaría de Educación, Ciencia, Tecnología e Innovación (SECTEI) of Mexico City for the postdoctoral fellowship SECTEI 177/2021. We thank F. Mazzarini, M.E. Rumpf, M. Poland, and an anonymous reviewer for their constructive criticism and valuable suggestions to improve the original manuscript.

References Cited

Agrawal, S., Guevara, M., and Verma, S.P., 2008, Tectonic discrimination of basic and ultrabasic volcanic rocks through log-transformed ratios of immobile trace elements: International Geology Review, v. 50, no. 12, p. 1057–1079, https://doi.org/10.2747/0020-6814.50.12.1057.

Alaniz-Álvarez, S., Nieto-Samaniego, A.F., and Ferrari, L., 1998, Effects of strain rate in the distribution of monogenetic and polygenetic volcanism in the Transmexican volcanic belt: Geology, v. 26, no. 7, p. 591–594, https://doi.org/10.1130/0091-7613(1998)026<0591:EOSRIT>2.3.CO;2.

Alaniz-Álvarez, S., and Nieto-Samaniego, Á.F., 2005, El sistema de fallas Taxco-San Miguel de Allende y la Faja Volcánica Transmexicana, dos fronteras tectónicas del centro de México activas durante el Cenozoico [The Taxco-San Miguel fault system, implications for the post-Eocene deformation of central Mexico]: Boletín conmemorativo del centenario de la Sociedad Geológica Mexicana [Bulletin of the Mexican Geological Society], v. 57, no. 1, p. 65–82, https://doi.org/10.18268/BSGM2005v57n1a4.

Alberico, I., Lirer, L., Petrosino, P., and Scandone, R., 2002, A methodology for the evaluation of long-term volcanic risk from pyroclastic flows in Campi Flegrei (Italy): Journal of Volcanology and Geothermal Research, v. 116, no. 1–2, p. 63–78, https://doi.org/10.1016/S0377-0273(02)00211-1.

Alva-Valdivia, L., 2005, Comprehensive paleomagnetic study of a succession of Holocene olivine-basalt flow—Xitle Volcano (Mexico) revisited: Earth, Planets, and Space, v. 57, no. 9, p. 839–853, at https://doi.org/10.1186/BF03351862.

Arce, J.L., Layer, P.W., Lassiter, J., Benowitz, J.A., Macías, J.L., and Ramírez-Espinosa, J., 2013, $^{40}Ar/^{39}Ar$ dating, geochemistry, and isotopic analyses of the Quaternary Chichinautzin volcanic field, south of México City—Implications for timing, effusion rate, and distribution of the volcanism: Bulletin of Volcanology, v. 75, no. 774, 25 p., https://doi.org/10.1007/s00445-013-0774-6.

Ban, N., Hasenaka, T., Delgado-Granados, H., and Takaoka, N., 1992, K-Ar ages of lavas from shield volcanoes in the Michoacán-Guanajuato volcanic field, Mexico: Geofísica Internacional, v. 31, no. 4, p. 467–473, https://doi.org/10.22201/igeof.00167169p.1992.31.4.1367.

Bartolini, S., Cappello, A., Martí, J., and Del Negro, C., 2013, QVAST—A new Quantum GIS plugin for estimating volcanic susceptibility: Natural Hazards and Earth System Sciences, v. 13, no. 11, p. 3031–3042, https://doi.org/10.5194/nhess-13-3031-2013.

Bartolini, S., Martí, J., Sobradelo, R., and Becerril, L., 2017, Probabilistic e-tools for hazard assessment and risk management, *in* Gottsmann, J., Neuberg, J., Scheu, B., eds, Volcanic unrest—From science to society: Cham, Switzerland, Springer, Advances in Volcanology, p. 47–62, https://doi.org/10.1007/11157_2017_14.

Bebbington, M., 2013, Assessing spatio-temporal eruption forecast in a monogenetic volcanic field: Journal of Volcanology and Geothermal Research, v. 252, p. 14–28, https://doi.org/10.1016/j.jvolgeores.2012.11.010.

Becerril, L., Cappello, A., Galindo, I., Neri, M., and Del Negro, C., 2013, Spatial probability distribution of future volcanic eruptions at El Hierro Island (Canary Islands, Spain): Journal of Volcanology and Geothermal Research, v. 257, p. 21–30, https://doi.org/10.1016/j.jvolgeores.2013.03.005.

Bemis, K.G., and Ferencz, M., 2017, Morphometric analysis of scoria cones—The potential for inferring process from shape: Special Publication - Geological Society of London, v. 446, no. 1, p. 61–100, https://doi.org/10.1144/SP446.9.

Benowitz, J.A., Layer, P.W., and Vanlaningham, S., 2014, Persistent long-term (c. 24 Ma) exhumation in the eastern Alaska range constrained by stacked thermochronology: Special Publication - Geological Society of London, v. 378, no. 1, p. 225–243, https://doi.org/10.1144/SP378.12.

Bevilacqua, A., Bursik, M., Patra, A., Pitman, E.B., and Till, R., 2017, Bayesian construction of a long-term vent opening probability map in the Long Valley volcanic region (CA, USA): Statistics in Volcanology, v. 3, p. 1–36, https://doi.org/10.5038/2163-338X.3.1.

Blanco, L.S.O., and Guilbaud, M.-N., 2025, Age and eruptive style of a cluster of Holocene monogenetic eruptions in the central part of the Sierra Chichinautzin Volcanic Field, Mexico—Implications for the monitoring of future eruptions, chap. H *of* Poland, M.P., Ort, M.H., Stovall, W.K., Vaughan, G.R., Connor, C.B., and Rumpf, M.E., eds., Distributed volcanism—Characteristics, processes, and hazards: U.S. Geological Survey Professional Paper 1890, ## p., https://doi.org/10.3133/pp1890H.

Bloomfield, K., 1975, A late-Quaternary monogenetic field in Central México: Geologische Rundschau, v. 64, no. 1, p. 476–497, https://doi.org/10.1007/BF01820679.

Böhnel, H., Morales, J., Caballero, C., Alva, L., McIntosh, G., González, S., and Sherwood, G., 1997, Variation of rock magnetic parameters and paleointensities over a single Holocene lava flow: Journal of Geomagnetism and Geoelectricity, v. 49, no. 4, p. 523–542, https://doi.org/10.5636/jgg.49.523.

Burbach, G.V., Frohlich, C., Pennington, W.D., and Matumoto, T., 1984, Seismicity and tectonics of the subducted Cocos Plate: Journal of Geophysical Research, v. 89, no. B9, p. 7719–7735, https://doi.org/10.1029/JB089iB09p07719.

Campos-Enríquez, J.O., Lermo-Samaniego, J.F., Antayhua-Vera, Y.T., Chavacán, M., and Ramón Márquez, V.M., 2015, The Aztlán Fault System—Control on the emplacement of the Chichinautzin Range volcanism, southern Mexico Basin, Mexico—Seismic and gravity characterization: Boletín de la Sociedad Geológica Mexicana, v. 67, no. 2, p. 315–335 [Bulletin of the Mexican Geological Society], https://doi.org/10.18268/BSGM2015v67n2a13.

Cañón-Tapia, E., and Walker, G.P.L., 2004, Global aspects of volcanism—The perspectives of "plate tectonics" and "volcanic systems": Earth-Science Reviews, v. 66, no. 1–2, p. 163–182, https://doi.org/10.1016/j.earscirev.2003.11.001.

Cebriá, J.M., Martiny, B.M., López-Ruiz, J., and Morán-Zenteno, D.J., 2011, The Parícutín calc-alkaline lavas—New geochemical and petrogenetic modelling constraints on the crustal assimilation process: Journal of Volcanology and Geothermal Research, v. 201, no. 1–4, p. 113–125, https://doi.org/10.1016/j.jvolgeores.2010.11.011.

Cervantes, P., and Wallace, P.J., 2003, Magma degassing and basaltic eruption styles—A case study of 2000 year BP Xitle volcano in central Mexico: Journal of Volcanology and Geothermal Research, v. 120, no. 3–4, p. 249–270, https://doi.org/10.1016/S0377-0273(02)00401-8.

Cervantes-Solano, M., Cifuentes-Nava, G., Caballero-Miranda, C.I., Goguitchaichvili, A., López-Loera, H., Delgado-Granados, H., Morales-Contreras, J., and Urrutia-Fucugauchi, J., 2019, Estudio magnético integral de flujos de lava del volcán Xitle—Implicaciones arqueológicas sobre el abandono de Cuicuilco: Boletín de la Sociedad Geológica Mexicana, v. 71, no. 2, p. 397–411, https://doi.org/10.18268/BSGM2019v71n2a10.

Chevrel, M.O., Siebe, C., Guilbaud, M.N., and Salinas, S., 2016, The AD 1250 El Metate shield volcano (Michoacán)—Mexico's most voluminous Holocene eruption and its significance for archaeology and hazards: The Holocene, v. 26, no. 3, p. 471–488, https://doi.org/10.1177/0959683615609757.

Connor, C.B., 1987, Structure of the Michoacán-Guanajuato volcanic field, México: Journal of Volcanology and Geothermal Research, v. 33, no. 1–3, p. 191–200, https://doi.org/10.1016/0377-0273(87)90061-8.

Connor, C.B., 1990, Cinder cone clustering in the Transmexican volcanic belt—Implications for structural and petrologic models: Journal of Geophysical Research, v. 95, B12, p. 19395–19405, https://doi.org/10.1029/JB095iB12p19395.

Connor, C.B., Condit, C.D., Crumpler, L.S., and Aubele, J.C., 1992, Evidence of regional structural controls on vent distribution—Springerville volcanic field, Arizona: Journal of Geophysical Research, v. 97, no. B9, p. 12349–12359, https://doi.org/10.1029/92JB00929.

Connor, C.B., and Hill, B.E., 1995, Three nonhomogeneous Poisson models for the probability of basaltic volcanism—Application to the Yucca Mountain region, Nevada: Journal of Geophysical Research, v. 100, no. B6, p. 10107–10125, https://doi.org/10.1029/95JB01055.

Connor, C.B., and Conway, F.M., 2000, Basaltic volcanic fields, *in* Sigurdsson, H., ed., Encyclopedia of Volcanoes: San Diego, Calif., Academic Press, p. 423–439.

Connor, C.B., Stamatakos, J.A., Ferrill, D.A., Hill, B.E., Ofoegbu, G.I., Conway, F.M., Sagar, B., and Trapp, J., 2000, Geologic factors controlling patterns of small-volume basaltic volcanism—Application to a volcanic hazards assessment at Yucca Mountain, Nevada: Journal of Geophysical Research, v. 105, no. B1, p. 417–432, https://doi.org/10.1029/1999JB900353.

Cordova, C., Martin Del Pozzo, A.L., and López Camacho, J., 1994, Paleolandforms and volcanic impact on the environment of prehistoric Cuicuilco, southern México City: Journal of Archaeological Science, v. 21, no. 5, p. 585–596, https://doi.org/10.1006/jasc.1994.1058.

Delaney, P.T., Pollard, D.D., Ziony, J.I., and McKee, E.H., 1986, Field relations between dikes and joints—Emplacement processes and paleostress analysis: Journal of Geophysical Research, v. 91, no. B5, p. 4920–4938, https://doi.org/10.1029/JB091iB05p04920.

Delgado-Granados, H., and Martin Del Pozzo, A.L., 1993, Pliocene to Holocene volcanic geology at the junction of Las Cruces, Chichinautzin and Ajusco ranges, southwest of México City: Geofísica Internacional, v. 32, no. 3, p. 511–522, https://doi.org/10.22201/igeof.00167169p.1993.32.3.526.

Di Traglia, F., Morelli, S., Casagli, N., and Garduño Monroy, V.H., 2014, Semi-automatic delimitation of volcanic edifice boundaries—Validation and application to the cinder cones of the Tancítaro-Nueva Italia region (Michoacán–Guanajuato volcanic field, Mexico): Geomorphology, v. 219, p. 152–160, https://doi.org/10.1016/j.geomorph.2014.05.002.

Dóniz-Páez, J., 2015, Volcanic geomorphological classification of the cinder cones of Tenerife (Canary Islands, Spain): Geomorphology, v. 228, p. 432–447, https://doi.org/10.1016/j.geomorph.2014.10.004.

Espinasa-Pereña, R., and Martin-Del Pozzo, A.L., 2006, Morphostratigraphic evolution of Popocatépetl volcano, México, *in* Siebe, C., Macías, J.L., and Aguirre-Díaz, G.J., eds., Neogene-Quaternary continental margin volcanism—A perspective from México: Geological Society of America Special Papers 402, p. 101–123, https://doi.org/10.1130/2006.2402(05).

Ferrari, L., Garduño, V.H., Pasquarè, G., and Tibaldil, A., 1994, Volcanic and tectonic evolution of central Mexico—Oligocene to present: Geofísica Internacional, v. 33, no. 1, p. 91–105, https://doi.org/10.22201/igeof.00167169p.1994.33.1.542.

Ferrari, L., López-Martinez, M., Aguirre-Díaz, G., and Carrasco-Núñez, G., 1999, Space-time patterns of Cenozoic arc volcanism in Central Mexico—From the Sierra Madre Occidental to the Mexican volcanic belt: Geology, v. 27, no. 4, p. 303–306, https://doi.org/10.1130/0091-7613(1999)027<0303:STPOCA>2.3.CO;2.

Ferrari, L., Conticelli, S., Vaggelli, G., Petrone, C., and Manetti, P., 2000, Late Miocene volcanism and intra-arc tectonics during the early development of the Trans-Mexican volcanic belt: Tectonophysics, v. 318, no. 1-4, p. 161–185, https://doi.org/10.1016/S0040-1951(99)00310-8.

Ferrari, L., Orozco-Esquivel, T., Manea, V., and Manea, M., 2012, The dynamic history of the Trans-Mexican volcanic belt and the Mexico subduction zone: Tectonophysics, v. 522–523, p. 122–149, https://doi.org/10.1016/j.tecto.2011.09.018.

Ferrari, L., Orozco-Esquivel, T., Bryan, S.E., López-Martínez, M., and Silva-Fragoso, A., 2018, Cenozoic magmatism and extension in western Mexico—Linking the Sierra Madre Occidental silicic large Igneous Province and the Comondú group with the Gulf of California rift: Earth-Science Reviews, v. 183, p. 115–152, https://doi.org/10.1016/j.earscirev.2017.04.006.

García-Palomo, A., Macías, J.L., Arce, J.L., Capra, L., Garduño, V.H., and Espíndola, J.M., 2002, Geology of Nevado de Toluca Volcano and surrounding areas, central Mexico: Boulder, Colo., Geological Society of America Map and Chart Series MCH089, 26 p.

García-Palomo, A., Zamorano, J.J., López-Miguel, C., Galván-García, A., Carlos-Valerio, V., Ortega, R., and Macías, J.L., 2008, El arreglo morfoestructural de la Sierra de Las Cruces, México central [The morphostructural arrangement of the Sierra de Las Cruces, central Mexico]: Revista Mexicana de Ciencias Geológicas [Mexican Journal of Geological Sciences], v. 25, p. 158–178, accessed September 17, 2025, at https://www.scielo.org.mx/scielo.php?script=sci_arttext&pid=S1026-87742008000100010.

Gómez–Tuena, A., Mori, L., Rincón–Herrera, N.E., Ortega–Gutiérrez, F., Solé, J., and Iriondo, A., 2008, The origin of a primitive trondhjemite from the Trans–Mexican volcanic belt and its implications for the construction of a modern continental arc: Geology, v. 36, no. 6, p. 471–474, https://doi.org/10.1130/G24687A.1.

Hasenaka, T., and Carmichael, I.S.E., 1985a, The cinder cones of Michoacán—Guanajuato, central Mexico—Their age, volume, distribution, and recharge rate: Journal of Volcanology and Geothermal Research, v. 25, no. 1–2, p. 105–124, https://doi.org/10.1016/0377-0273(85)90007-1.

Hasenaka, T., and Carmichael, I.S.E., 1985b, A compilation of location, size, and geomorphological parameters of volcanoes of the Michoacán-Guanajuato volcanic field, central Mexico: Geofísica Internacional, v. 24, no. 4, p. 577–607, https://doi.org/10.22201/igeof.00167169p.1985.24.4.2179.

Hasenaka, T., and Carmichael, I.S.E., 1987, The cinder cones of Michoacán-Guanajuato, central Mexico—Petrology and chemistry: Journal of Petrology, v. 28, no. 2, p. 241–269, https://doi.org/10.1093/petrology/28.2.241.

Hasenaka, T., Ban, M., and Delgado-Granados, H., 1994, Contrasting volcanism in the Michoacán-Guanajuato volcanic field, central Mexico—Shield volcanoes vs. cinder cones: Geofísica Internacional, v. 33, no. 1, p. 125–138, https://doi.org/10.22201/igeof.00167169p.1994.33.1.544.

Havskov, J., 1982, The earthquake swarm of February 1981 in Mexico City: Geofísica Internacional, v. 21, no. 2, p. 157–175, https://doi.org/10.22201/igeof.00167169p.1982.21.2.909.

Hooper, D.M., 1995, Computer-simulation models of scoria cone degradation in the Colima and Michoacán-Guanajuato volcanic field, Mexico: Geofísica Internacional, v. 34, no. 3, p. 321–340, https://doi.org/10.22201/igeof.00167169p.1995.34.3.727.

Inbar, M., Gilichinsky, M., Melekestsev, M., Melnikov, D., and Zaretskaya, N., 2011, Morphometric and morphological development of Holocene cinder cones—A field and remote sensing study in the Tolbachik volcanic field, Kamchatka: Journal of Volcanology and Geothermal Research, v. 201, no. 1–4, p. 301–311, https://doi.org/10.1016/j.jvolgeores.2010.07.013.

Jaimes-Viera, M.C., Martin del Pozzo, A.L., Layer, P.W., Benowitz, J.A., and Nieto-Torres, A., 2018, Timing the evolution of a monogenetic volcanic field—Sierra Chichinautzin, central Mexico: Journal of Volcanology and Geothermal Research, v. 356, p. 225–242, https://doi.org/10.1016/j.jvolgeores.2018.03.013.

Johnson, C., and Harrison, C., 1989, Tectonics and volcanism in central Mexico—A landsat thematic mapper perspective: Remote Sensing of Environment, v. 28, p. 273–286, https://doi.org/10.1016/0034-4257(89)90119-3.

Johnson, C.A., and Harrison, C.G.A., 1990, Neotectonics in central Mexico: Physics of the Earth and Planetary Interiors, v. 64, no. 2–4, p. 187–210, https://doi.org/10.1016/0031-9201(90)90037-X.

Johnson, E.R., Wallace, P.J., Cashman, K.V., Delgado-Granados, H.D., and Kent, A.J., 2008, Magmatic volatile contents and degassing-induced crystallization at Volcán Jorullo, Mexico—Implications for melt evolution and the plumbing systems of monogenetic volcanoes: Earth and Planetary Science Letters, v. 269, no. 3–4, p. 478–487, https://doi.org/10.1016/j.epsl.2008.03.004.

Jolly, R., and Sanderson, D., 1997, A Mohr circle construction for the opening of a pre-existing fracture: Journal of Structural Geology, v. 19, no. 6, p. 887–892, https://doi.org/10.1016/S0191-8141(97)00014-X.

Kiyosugi, K., Connor, C.B., Zhao, D., Connor, L.J., and Tanaka, K., 2010, Relationships between volcano distribution, crustal structure, and P-wave tomography—An example from the Abu Monogenetic volcano group, SW Japan: Bulletin of Volcanology, v. 72, no. 3, p. 331–340, https://doi.org/10.1007/s00445-009-0316-4.

Kósik, S., Bebbington, M., and Németh, K., 2020, Spatio-temporal hazard estimation in the central silicic part of Taupo volcanic zone, New Zealand, based on small to medium volume eruptions: Bulletin of Volcanology, v. 82, no. 50, p. 1–15, https://doi.org/10.1007/s00445-020-01392-6.

Kurokawa, K., Otsuki, K.,and Hasenaka, T., 1995, Tectonic stress field and fractal distributions of volcanoes in the Michoacán-Guanajuato region of the Mexican volcanic belt: Geofísica Internacional, v. 34, no. 3, p. 309–320, https://doi.org/10.22201/igeof.00167169p.1995.34.3.726.

Layer, P.W., Hall, C.M., and York, D., 1987, The derivation of $^{40}Ar/^{39}Ar$ age spectra of single grains of hornblende and biotite by laser step heating: Geophysical Research Letters, v. 14, no. 7, p. 757–760, https://doi.org/10.1029/GL014i007p00757.

Le Corvec, N., Spörli, K.B., Rowland, J., and Lindsay, J., 2013, Spatial distribution and alignments of volcanic centers—Clues to the formation of monogenetic volcanic fields: Earth-Science Reviews, v. 124, p. 96–114, https://doi.org/10.1016/j.earscirev.2013.05.005.

Legrand, D., Perton, M., Macías, J.L., Siebe, C., Pacheco, J., Chacón, F., Lermo, J., Quintanar, L., and Cisneros, G., 2023, Repeated seismic swarms near Paricutin volcano—Precursors to the birth of a new monogenetic volcano in the Michoacán-Guanajuato volcanic field, México?: Bulletin of Volcanology, v. 85, no. 30, 15 p., https://doi.org/10.1007/s00445-023-01645-0.

Luhr, J.F., and Carmichael, I.S.E., 1985, Jorullo Volcano, Michoacán, Mexico (1759–1774)—The earliest stages of fractionation in calc-alkaline magmas: Contributions to Mineralogy and Petrology, v. 90, no. 2-3, p. 142–161, https://doi.org/10.1007/BF00378256.

Márquez, A., Verma, S.P., Anguita, F., Oyarzum, R., and Brandle, J.L., 1999, Tectonics and volcanism of Sierra Chichinautzin—Extension at the front of the central Trans-Mexican volcanic belt: Journal of Volcanology and Geothermal Research, v. 93, no. 1–2, p. 125–150, https://doi.org/10.1016/S0377-0273(99)00085-2.

Martin Del Pozzo, A.L., 1981, Vulcanología de la zona Tetequillo-Xicomulco [Volcanology of the Tetequillo-Xicomulco area]: Memorias de la Unión Geofísica Mexicana [Memoirs of the Mexican Geophysical Union], v. 1, no. 4A, 7 p.

Martin Del Pozzo, A.L., 1982, Monogenetic volcanism in Sierra Chichinautzin, Mexico: Bulletin of Volcanology, v. 45, no. 1, p. 9–24, https://doi.org/10.1007/BF02600386.

Martin Del Pozzo, A.L., 1990, Geoquímica y Paleomagnetismo de la Sierra Chichinautzin [Geochemistry and Paleomagnetism of the Sierra Chichinautzin]: Mexico City, Mexico, Universidad Nacional Autónoma de México, Ph.D. dissertation, 235 p.

Martin Del Pozzo, A.L., Córdoba, C., and López, J., 1997, Volcanic impact on the southern basin of Mexico during the Holocene: Quaternary International, v. 43–44, p. 181–190, https://doi.org/10.1016/S1040-6182(97)00034-7.

Martínez-Serrano, R., Schaaf, P., Solís-Pichardo, G., Hernández-Bernal, M.S., Hernández-Terviño, T., Morales-Contreras, J.J., and Macías, J.L., 2004, Sr, Nd and Pb isotope and geochemical data from the Quaternary Nevado de Toluca volcano, a source of recent adakitic magmatism, and the Tenango volcanic field, Mexico: Journal of Volcanology and Geothermal Research, v. 138, no. 1–2, p. 77–110, https://doi.org/10.1016/j.jvolgeores.2004.06.007.

Mazzarini, F., Ferrari, L., and Isola, I., 2010, Self-similar clustering of cinder cones and crust thickness in the Michoacan-Guanajuato and Sierra de Chichinautzin volcanic fields, Trans-Mexican volcanic belt: Tectonophysics, v. 486, no. 1–4, p. 55–64, https://doi.org/10.1016/j.tecto.2010.02.009.

Mazzarini, F., Le Corvec, N., Isola, I., and Favalli, M., 2016, Volcanic field elongation, vent distribution, and tectonic evolution of a continental rift—The main Ethiopian rift example: Geosphere, v. 12, no. 3, p. 706–720, https://doi.org/10.1130/GES01193.1.

McBirney, A.R., Taylor, H.P., and Armstrong, R.L., 1987, Paricutin reexamined—A classic example of crustal assimilation in calc-alkaline magma: Contributions to Mineralogy and Petrology, v. 95, no. 1, p. 4–20, https://doi.org/10.1007/BF00518026.

McDougall, I., and Harrison, T.M., 1999, Geochronology and Thermochronology by the $^{40}Ar/^{39}Ar$ method (2d ed.): New York, Oxford University Press, 269 p. https://doi.org/10.1093/oso/9780195109207.001.0001.

Mitchell, A., and Griffin, L.S., 2005, The ESRI Guide to GIS Analysis (2d ed.). ESRI Press.

Morales, J., Goguitchaichvili, A., and Urrutia-Fucugauchi, J., 2014, A rock-magnetic and paleointensity study of some Mexican volcanic lava flows during the latest Pleistocene to Holocene: Earth, Planets, and Space, v. 53, no. 9, p. 893–902, https://doi.org/10.1186/BF03351686.

Morales-Casique, E., Arce Saldaña, J.L., Lezama Campos, J.L., and Escolero Fuentes, O., 2018, Análisis de la estratigrafía y las características hidrogeológicas de los estratos profundos que conforman el subsuelo de la cuenca de México a partir de la perforación de dos pozos profundos, uno a 2000 m y otro a 1570 m denominados Agrícola Oriental no. 2B y 2C [Analysis of the stratigraphy and hydrogeological characteristics of the deep strata that make up the subsoil of the basin of México from the drilling of two deep wells, one at 2000 m and other at 1570 m, called Agrícola Oriental no. 2B and 2C]: Boletín del Instituto de Geología [Bulletin of the Institute of Geology], no. 121, 60 p.

Muirhead, J.D., Kattenhorn, S.A., and Le Corvec, N., 2015, Varying styles of magmatic strain accommodation across the East African Rift: Geochemistry, Geophysics, Geosystems, v. 16, no. 8, p. 2775–2795, https://doi.org/10.1002/2015GC005918.

Murphy, G.P., 1986, The chronology, pyroclastic stratigraphy, and petrology of the Valle de Santiago maar field, central Mexico: Berkeley, California, University of California, Master's thesis, 55 p.

Negendank, J.F., 1972, Volcanics of the valley of México—Petrography of the volcanics: Neues Jahrbuch für Mineralogie. Abhandlungen, v. 116, p. 308–320.

Nieto-Torres, A., and Martin Del Pozzo, A.L., 2019, Spatio-temporal hazard assessment of a monogenetic volcanic field, near México City: Journal of Volcanology and Geothermal Research, v. 371, p. 46–58, https://doi.org/10.1016/j.jvolgeores.2019.01.006.

Nieto-Torres, A., Martin Del Pozzo, A.L., Groppelli, G., and Jaimes-Viera, M.C., 2023, Risk scenarios for a future eruption in the Chichinautzin monogenetic volcanic field, south México City: Journal of Volcanology and Geothermal Research, v. 433, 25 p., https://doi.org/10.1016/j.jvolgeores.2022.107733.

Nixon, G.T., 1982, The relationship between Quaternary volcanism in central Mexico and the seismicity and structure of subducted ocean lithosphere: Geological Society of America Bulletin, v. 93, no. 6, p. 514–523, https://doi.org/10.1130/0016-7606(1982)93<514:TRBQVI>2.0.CO;2.

Norini, G., Groppelli, G., Lagmay, A.M.F., and Capra, L., 2006, Recent left-oblique slip faulting in central Trans-Mexican volcanic belt—Seismic hazard and geodynamic implications: Tectonics, v. 25, no. 4, 21 p., https://doi.org/10.1029/2005TC001877.

Orozco y Berra, M., 1854, Diccionario universal de historia y geografía, México [Universal dictionary of history and geography, Mexico]: Tipografía de Rafael/Librería de Andrade [Rafael Typography/Andrade Bookstore], v. 4, p. 453.

Ownby, S.E., Delgado-Granados, H.D., Lange, R.A., and Hall, C.M., 2007, Volcán Tancítaro, Michoacán, Mexico, $^{40}Ar/^{39}Ar$ constraints on its history of sector collapse: Journal of Volcanology and Geothermal Research, v. 161, no. 1–2, p. 1–14, https://doi.org/10.1016/j.jvolgeores.2006.10.009.

Ownby, S.E., Lange, R.A., Hall, C.M., and Delgado-Granados, H., 2011, Origin of andesite in the deep crust and eruption rates in the Tancítaro-Nueva Italia region of the central Mexican arc: Geological Society of America Bulletin, v. 123, no. 1–2, p. 274–294, https://doi.org/10.1130/B30124.1.

Pardo, M., and Suárez, G., 1995, Shape of the subducted Rivera and Cocos Plates in southern Mexico—Seismic and tectonic implications: Journal of Geophysical Research, v. 100, no. B7, no. B7, p. 12357–12373, https://doi.org/10.1029/95JB00919.

Pasquarè, G., Garduño Monroy, V.H., Tibaldi, A., and Ferrari, L., 1990, Migrazione di un arco vulcanico continentale—Dalla Sierra Madre Occidentale all "arco Vulcanico Messicano" [Migration of a continental volcanic arc—From the Sierra Madre Occidental to the "Mexican volcanic arc"]: Società Geologica Italiana [Italian Geological Society], v. 45, p. 939–946.

Pasquarè, G., Ferrari, L., Garduño Monroy, V.H., Tibaldi, A., and Vezzoli, L., 1991, Geologic map of the central Mexican Volcanic Belt, states of Guanajuato and Michoacán, Mexico: Geological Society of America Map and Chart Series MCH072, 1 sheet, scale 1:300,000.

Paton, D., Johnston, D., Gough, J., Dowrick, D., Manville, V., Daly, M., Batistich, T., and Baddon, L., 1999, Auckland Volcanic Risk Project—Stage 2: Auckland Regional Council Technical Publication 126, 99 p.

Paulsen, T.S., and Wilson, T.J., 2010, New criteria for systematic mapping and reliability assessment of monogenetic volcanic vent alignments and elongate volcanic vents for crustal stress analyses: Tectonophysics, v. 482, no. 1–4, p. 16–28, https://doi.org/10.1016/j.tecto.2009.08.025.

Pérez-Campos, X., Kim, Y., Husker, A., Davis, P.M., Clayton, R.W., Iglesias, A., Pacheco, J.F., Singh, S.K., Manea, V.C., and Gurnis, M., 2008, Horizontal subduction and truncation of the Cocos Plate beneath central Mexico: Geophysical Research Letters, v. 35, no. 18, 6 p., https://doi.org/10.1029/2008GL035127.

Pioli, L., Erlund, E., Johnson, E., Cashman, K., Wallace, P., Rosi, M., and Delgado-Granados, H., 2008, Explosive dynamics of violent Strombolian eruptions—The eruption of Parícutin Volcano 1943–1952 (Mexico): Earth and Planetary Science Letters, v. 271, no. 1–4, p. 359–368, https://doi.org/10.1016/j.epsl.2008.04.026.

Renne, P.R., Deino, A.L., Walter, R.C., Turrin, B.D., Swisher, C.C., III, Becker, T.A., Curtis, G.H., Sharp, W.D., and Jaouni, A.R., 1994, Intercalibration of astronomical and radioisotopic time: Geology, v. 22, no. 9, p. 783–786, https://doi.org/10.1130/0091-7613(1994)022<0783:IOAART>2.3.CO;2.

Renne, P.R., Mundil, R., Balco, G., Min, K., and Ludwig, K., 2010, Joint determination of ^{40}K decay constants and the $^{40}Ar^*/^{40}K$ for the Fish Canyon sanidine standard and improved accuracy for $^{40}Ar/^{39}Ar$ geochronology: Geochimica et Cosmochimica Acta, v. 74, no. 18, p. 5349–5367, https://doi.org/10.1016/j.gca.2010.06.017.

Reyes-Guzmán, N., Siebe, C., Chevrel, M.O., Pereira, G., Mahgoub, A.N., and Böhnel, H., 2023, Holocene volcanic eruptions of the Malpaís de Zacapu and its pre-Hispanic settlement history: Ancient Mesoamerica, v. 34, no. 3, p. 712–727, https://doi.org/10.1017/S095653612100050X.

Rose, W.I., Jr., 1973, Pattern and mechanism of volcanic activity at the Santiaguito volcanic dome, Guatemala: Bulletin of Volcanology, v. 37, no. 1, p. 73–94, https://doi.org/10.1007/BF02596881.

Rooney, T.O., Bastow, I.D., and Keir, D., 2011, Insights into extensional processes during magma assisted rifting—Evidence from aligned scoria cones: Journal of Volcanology and Geothermal Research, v. 201, no. 1–4, p. 83–96, https://doi.org/10.1016/j.jvolgeores.2010.07.019.

Runge, M.G., Bebbington, M.S., Cronin, S.J., Lindsay, J.M., Kenedi, C.L., and Moufti, M.R.H., 2014, Vents to events—Determining an eruption event record from volcanic vent structures for the Harrat Rahat, Saudi Arabia: Bulletin of Volcanology, v. 76, no. 804, p. 76, https://doi.org/10.1007/s00445-014-0804-z.

Scandone, R., 1979, Preliminary evaluation of the volcanic hazard in the southern valley of México: Geofísica Internacional, v. 18, no. 1, p. 21–35, at https://doi.org/10.22201/igeof.00167169p.1979.18.1.1092.

Siebe, C., Rodríguez-Lara, V., Schaaf, P., and Abrams, M., 2004, Geochemistry, Sr–Nd isotope composition, and tectonic setting of Holocene Pelado, Guespalapa and Chichinautzin scoria cones, south of México City: Journal of Volcanology and Geothermal Research, v. 130, no. 3–4, p. 197–226, https://doi.org/10.1016/S0377-0273(03)00289-0.

Siebe, C., Salinas, S., Arana-Salinas, L., Macías, J.L., Gardner, J., and Bonasia, R., 2017, The ~23,500y ^{14}C BP white pumice plinian eruption and associated debris avalanche and Tochimilco lava flow of Popocatépetl volcano, México: Journal of Volcanology and Geothermal Research, v. 333–334, p. 66–95, https://doi.org/10.1016/j.jvolgeores.2017.01.011.

Sigtryggsdóttir, F.G., Hrafnsdóttir, H., Steingrímsson, J.H., and Guðmundsson, A., 2025, Experience in diverting and containing lava flow by barriers constructed from in situ material during the 2021 Geldingardalir volcanic eruption: Bulletin of Volcanology, v. 87, no. 28, 23 p., https://doi.org/10.1007/s00445-025-01806-3.

Singh, S.K., Anderson, J.G., and Rodríguez, M., 1998, Triggered seismicity in the valley of Mexico from major Mexican earthquakes: Geofísica Internacional, v. 37, no. 1, p. 3–15, https://doi.org/10.22201/igeof.00167169p.1998.37.1.2155.

Smith, I.E.M., and Németh, K., 2017, Source to surface model of monogenetic volcanism—A critical review, *in* Németh, K., Carrasco-Núñez, G., Aranda-Gómez, J.J., and Smith, I.E.M., eds., Monogenetic Volcanism—London: Geological Society of London, Special Publications 446, p. 1–28., https://doi.org/10.1144/SP446.14.

Sobradelo, R., Bartolini, S., and Martí, J., 2014, HASSET—A probability event tree tool to evaluate future volcanic scenarios using Bayesian inference; presented as a plug-in for QGIS: Bulletin of Volcanology, v. 76, no. 770, 15 p., https://doi.org/10.1007/s00445-013-0770-x.

Soria-Caballero, D.C., Garduño-Monroy, V.H., Alcalá, M., Velázquez-Bucio, M.M., and Grassi, L., 2019, Evidence for Quaternary seismic activity of the La Alberca-Teremendo Fault, Morelia region, Trans-Mexican volcanic belt: Revista Mexicana de Ciencias Geológicas, v. 36, no. 2, p. 242–258, https://doi.org/10.22201/cgeo.20072902e.2019.2.1092.

Straub, S.M., and Martin Del Pozzo, A.L., 2001, The significance of phenocryst diversity in tephra from recent eruptions at Popocatépetl volcano (central Mexico): Contributions to Mineralogy and Petrology, v. 140, no. 4, p. 487–510, https://doi.org/10.1007/PL00007675.

Straub, S.M., LaGatta, A.B., Martin Del Pozzo, A.L., and Langmuir, C., 2008, Evidence from high-Ni olivines for a hybridized peridotite/pyroxenite source for orogenic andesites from the central Mexican volcanic belt: Geochemistry, Geophysics, Geosystems, v. 9, no. 3, p. 1–33, https://doi.org/10.1029/2007GC001583.

Suter, M., Martínez, M.L., Legorreta, O.Q., and Martínez, M.C., 2001, Quaternary intra-arc extension in the central Trans-Mexican volcanic belt: Geological Society of America Bulletin, v. 113, no. 6, p. 693–703, https://doi.org/10.1130/0016-7606(2001)113<0693:QIAEIT>2.0.CO;2.

Takada, A., 1994, The influence of regional stress and magmatic input on styles of monogenetic and polygenetic volcanism: Journal of Geophysical Research, v. 99, no. B7, no. B7, p. 13563–13573, https://doi.org/10.1029/94JB00494.

Universidad Nacional Autónoma de Mexico-Servicio Sismológico Nacional [UNAM-SSN], 2023, Catálogo de sismos [Earthquake catalogue]: Universidad Nacional Autónoma de México, Instituto de Geofísica, Servicio Sismológico Nacional, México, accessed September 17, 2025, at http://www2.ssn.unam.mx:8080/catalogo/#.

Urrutia-Fucugauchi, J., and the Urrutia-Fucugauchi, 1996, Palaeomagnetic study of the Xitle-Pedregal de San Angel lava flow, southern basin of Mexico: Physics of the Earth and Planetary Interiors, v. 97, no. 1–4, p. 177–196, https://doi.org/10.1016/0031-9201(95)03136-7.

Urrutia-Fucugauchi, J., and Flores-Ruiz, J.H., 1996, Bouguer gravity anomalies and regional crustal structure in central Mexico: International Geology Review, v. 38, no. 2, p. 176–194, https://doi.org/10.1080/00206819709465330.

Urrutia-Fucugauchi, J., Goguitchaichvili, A., Pérez-Cruz, L., and Morales, J., 2016, Archaeomagnetic dating of the eruption of Xitle Volcano, basin of Mexico—Implications for the Mesoamerican centers of Cuicuilco and Teotihuacan: Arqueología Iberoamericana, v. 30, p. 23–29, https://doi.org/10.5281/zenodo.1317021.

Valentine, G.A., and Connor, C., 2015, Basaltic volcanic fields, chap. 23 *of* Sigurdsson, H., ed., The Encyclopedia of Volcanoes (Second Edition): Academic Press, p. 423-439, https://doi.org/10.1016/B978-0-12-385938-9.00023-7.

Verma, S., 2000, Geochemistry of the subducting Cocos Plate and the origin of subduction unrelated mafic volcanism at the front of the central Mexican volcanic belt: Geological Society of America Special Papers 334, p. 1–28., https://doi.org/10.1130/0-8137-2334-5.195.

Wallace, P., and Carmichael, I.S.E., 1999, Quaternary volcanism near the valley of Mexico—Implications for subduction zone magmatism and the effects of crustal thickness variations on primitive magma compositions: Contributions to Mineralogy and Petrology, v. 135, no. 4, p. 291–314, https://doi.org/10.1007/s004100050513.

Wessa, P., 2023, Hierarchical Clustering, version 1.0.5, in Free Statistics Software, version 1.2.1: Office for Research Development and Education, accessed August 14, 2024, at https://www.wessa.net/rwasp_hierarchicalclustering.wasp.

Williams, H., 1956, Volcanoes of the Paricutin region, Mexico, chap. B *of* Segerstrom, K.K., Williams, H., Wilcox, R.E., Foshag, W.P., and Gonzales, J.R., eds., Geologic investigations in the Parícutin area, Mexico: U.S. Geological Survey Bulletin 965, p. 162–279., https://doi.org/10.3133/b965.

Wood, C.A., 1980, Morphometric evolution of cinder cones: Journal of Volcanology and Geothermal Research, v. 7, no. 3–4, p. 387–413, https://doi.org/10.1016/0377-0273(80)90040-2.

York, D., Hall, C.M., Yanase, Y., Hanes, J.A., and Kenyon, W.J., 1981, $^{40}Ar/^{39}Ar$ dating of terrestrial minerals with a continuous laser: Geophysical Research Letters, v. 8, no. 11, p. 1136–1138, https://doi.org/10.1029/GL008i011p01136.

Moffett Field Publishing Service Center
Manuscript approved September 4, 2025
Edited by Hayden M. Chaisson
Illustration support by Katie Sullivan
Layout by Cory Hurd

ISSN 2330-7102 (online)
https://doi.org/10.3133/pp1890I